NASA TECHNICAL NOTE

NASA TN D-7207

NASA TN D-7207

COOLANT-SIDE HEAT-TRANSFER RATES FOR A HYDROGEN-OXYGEN ROCKET AND A NEW TECHNIQUE FOR DATA CORRELATION

by Ralph L. Schacht and Richard J. Quentmeyer

Lewis Research Center
Cleveland, Ohio 44135

NATIONAL AERONAUTICS AND SPACE ADMINISTRATION • WASHINGTON, D. C. • MARCH 1973

1. Report No.	2. Government Accession No.	3. Recipient's Catalog No.
NASA TN D-7207		

4. Title and Subtitle	5. Report Date
COOLANT-SIDE HEAT-TRANSFER RATES FOR A HYDROGEN-OXYGEN ROCKET AND A NEW TECHNIQUE FOR DATA CORRELATION	March 1973
	6. Performing Organization Code

7. Author(s)	8. Performing Organization Report No.
Ralph L. Schacht and Richard J. Quentmeyer	E-7204
	10. Work Unit No.
	503-35

9. Performing Organization Name and Address	11. Contract or Grant No.
Lewis Research Center National Aeronautics and Space Administration Cleveland, Ohio 44135	
	13. Type of Report and Period Covered
12. Sponsoring Agency Name and Address	Technical Note
National Aeronautics and Space Administration Washington, D.C. 20546	14. Sponsoring Agency Code

15. Supplementary Notes

16. Abstract

An experimental investigation was conducted at the NASA Lewis Research Center to determine the coolant-side heat-transfer coefficients for a liquid-hydrogen-cooled, hydrogen-oxygen rocket thrust chamber. Heat-transfer rates were determined from measurements of local hot-gas wall temperature, local coolant temperature, and local coolant pressure. A correlation incorporating an integration technique for the transport properties needed near the pseudocritical temperature of liquid hydrogen gives a satisfactory prediction of hot-gas wall temperatures.

17. Key Words (Suggested by Author(s))	18. Distribution Statement
Heat transfer Hydrogen-oxygen rocket engines Nuclear rockets	Unclassified - unlimited

19. Security Classif. (of this report)	20. Security Classif. (of this page)	21. No. of Pages	22. Price*
Unclassified	Unclassified	47	$3.00

* For sale by the National Technical Information Service, Springfield, Virginia 22151

COOLANT-SIDE HEAT-TRANSFER RATES FOR A HYDROGEN-OXYGEN ROCKET AND A NEW TECHNIQUE FOR DATA CORRELATION

by Ralph L. Schacht and Richard J. Quentmeyer

Lewis Research Center

SUMMARY

An experimental investigation was conducted at the NASA Lewis Research Center to determine the coolant-side heat-transfer rates in a liquid-hydrogen-cooled rocket thrust chamber, where the coolant was near the pseudocritical temperature region. Heat-transfer rates were determined from measurements of local hot-gas wall temperature, and local coolant temperature and pressure. A correlation of the form $StPr^{0.6} = 0.023\ Re^{-0.2}$, where all transport properties are evaluated by an integration technique, gave a reasonable correlation of the test data. (St is Stanton number, Pr is Prandtl number, and Re is Reynolds number.) The main advantage of this technique is that the correlation does not need to be altered in going from the subcritical to the supercritical temperature regime. No corrections are needed for low bulk temperatures, and standard entrance corrections can be used. Ito's curvature correction gave about the right magnitude for the curvature enhancement term that is needed in the throat region.

INTRODUCTION

The design of high-performance, convectively cooled, chemical and nuclear rocket systems requires accurate knowledge of the heat flow across the gas boundary on the hot-gas side of the coolant tubes and across the liquid boundary on the coolant-side of the tubes. High-performance rocket thrust chambers have high heat fluxes and high wall temperatures. Analytical and experimental studies were initiated at the NASA Lewis Research Center to develop the engineering and technology required to design cooling systems for these rocket systems. The experimental technique chosen was a gaseous-hydrogen, liquid-oxygen rocket that had a completely independent, liquid-hydrogen cooling system. This produced a design that gave high heat fluxes and allowed the variables on the coolant side to be varied independently of those on the hot-gas side. The coolant

tubes were designed to pass liquid-hydrogen flows that would be consistent with a nuclear-rocket thrust chamber design. This requires much greater quantities of hydrogen than those used with a regeneratively cooled, chemical, hydrogen-oxygen rocket, where hydrogen normally is about 15 weight percent of the total propellant. The end result is that the liquid hydrogen is at pressures higher than critical throughout the passage, and the temperature is below critical at the inlet and above critical at the outlet of the coolant passage. Thus, the liquid hydrogen in the coolant passage always has to pass through the pseudocritical temperature. Although a phase change does not occur at supercritical pressures, large changes in the transport properties do occur with very small changes in temperature near the pseudocritical temperature. Reference 1 gives a review of forced-convection heat transfer to fluids at supercritical pressures and points out the present unsatisfactory state of empirical correlations and semiempirical theories.

The thrust chamber used for this study had the same geometry as the thrust chamber used in references 2 and 3, which reported the hot-gas side heat-transfer coefficients. Thus, the only unknown heat-transfer quantities for this configuration were those on the coolant side.

Investigations and correlations of coolant-side heat transfer in rocket nozzles have been reported in references 4 to 11. In reference 4, the hydrogen coolant temperature is above the pseudocritical temperature in a very short distance in the coolant passage. A normal correlation of the form $Nu = 0.025\ Re^{0.8}Pr^{0.333}$ (symbols are defined in appendix A) seems to be a reasonable correlation for the major part of the coolant passage. Reference 5 also found a correlation of this type to be reasonable for straight tubes. Reference 6 gives a correlation for 4600 experimental heat-transfer coefficients for hydrogen flowing through straight tubes. Reference 7 gives a correlation commonly used in predicting heat-transfer coefficients in coolant passages of regeneratively cooled, nuclear rocket nozzles. References 8 and 9 found this correlation had to be modified by a proportionality constant which varied nonlinearly with coolant temperature. Reference 10 gives a correlation that works well with supercritical water and carbon dioxide. In reference 11, Deissler suggests using a special reference temperature for finding the transport properties.

All these correlations have differences, and each seems to work well for just one particular set of conditions. Therefore, there was an apparent need for measurements of local hot-gas wall temperature, and local liquid-hydrogen temperature and pressure in actual rocket firings where all factors such as curvature, asymmetric heating, tapered tubes, liquid-hydrogen pressures above critical, and liquid hydrogen temperatures that pass through the pseudocritical temperature are present. Thus, measuring the actual local effects instead of the overall effects was deemed necessary.

In this investigation, five axial measuring locations on two coolant tubes were installed on several rocket thrust chambers, and tests were run at chamber pressures of

2.07 and 3.1 meganewtons per square meter absolute (300 and 450 psia) with various coolant pressures and flows. Local, forced-convection, heat-transfer coefficients for supercritical hydrogen flowing inside coolant passages were calculated from the experimental data.

Based on the results of this investigation, a correlation was obtained for fully developed flow. The correlation incorporates an integration technique for the transport properties needed near the pseudocritical temperature of liquid hydrogen.

APPARATUS AND EXPERIMENTAL PROCEDURE

Rocket Design

A liquid-hydrogen cooled, hydrogen-oxygen rocket was used in the experiments to obtain hot-gas wall temperatures and liquid-hydrogen pressures and temperatures at five axial locations. The thrust chamber (fig. 1) had contraction and expansion area ratios of 4.64. The length of the combustion chamber from the injector to the throat was 36.8 centimeters (14.5 in.). The characteristic length L^* was 137 centimeters (54 in.). The throat diameter was 12.7 centimeters (5 in.).

A coaxial injector (fig. 2) was used with liquid oxygen and gaseous hydrogen as the propellants. The injector had 234 injector elements uniformly spaced in a dish-shaped, porous Rigimesh faceplate made of AISI-304 stainless-steel material (2.6 elements per 6.45 cm^2 or 1 $in.^2$). The chamber and injector were designed specifically to ensure stable engine operation and uniform distribution of mass flux and temperature to eliminate striation effects. Reference 3, which used the same injector geometry and chamber design, made a detailed study of the hot-gas-side, heat-transfer coefficients. Six circumferential measuring stations in that investigation showed a variation of ±20 percent in the hot-gas-side, heat-transfer coefficient in the chamber, which is considered a small variation for a chemical-rocket system.

The coolant passages were designed for nuclear type flows (all the propellant for a nuclear nozzle usually passes through the coolant passages) with the use of simple correlations of the type $St^*Pr^{*m} = CRe^{*n}$ for both the hot-gas side and the coolant side. For the hot-gas side, $C = 0.026$, $m = 0.7$, and $n = -0.2$. For the coolant side, $C = 0.023$, $m = 0.6$, and $n = -0.2$. The design had 150 coolant tubes made of AISI-347 stainless-steel material. The tube wall thickness was 0.0254 centimeter (0.010 in.). Later engines were built with tubes having 0.03048-centimeter (0.012-in.) walls. The geometric details of the tube are given in table I.

Instrumentation

Figure 3 indicates the locations of five axial instrumentation stations in the rocket thrust chamber. These instrumentation stations are located at design axial stations 2, 4, 7, 10, and 14 (see table I). These locations were used on two coolant tubes (a and b) that were 180° apart.

At each instrumentation station, four hot-gas-side thermocouples were installed. The hot-gas-side wall temperature was obtained from Platinel/stainless-steel thermocouples spot-welded to the stainless-steel tube surface and plated over with copper or nickel. The plating was faired in, so that the flow of the hot gases over the surface was smooth. Reference 12 gives a detailed discussion of the installation of these miniaturized thermocouples. At a position 1.27 centimeters (0.5 in.) upstream and 1.27 centimeters (0.5 in.) downstream of these instrument locations, Chromel-constantan thermocouples were installed in the coolant passage to obtain the liquid-hydrogen temperature. A liquid-nitrogen bath was installed on the thrust chamber at each instrument location. This allowed all connections to be made in an area of constant temperature, which served as a reference temperature, and minimized the lengths of the small thermocouple wire needed. All wire from the bath to readout was copper. The miniaturization of these thermocouples resulted in short operating lives, but because of redundancy, they provided the needed data. A static-pressure tap was installed 0.762 centimeter (0.3 in.) upstream of the wall-temperature measurement. These readings plus the pressures and temperatures measured at the inlet and outlet manifolds gave the liquid-hydrogen pressure and temperature distributions through the passage. Three platinum resistance thermometers were used in the inlet manifold, and four in the outlet manifold.

Data Recording

Propellant flows, chamber pressure, coolant flows, wall temperatures, coolant pressures, and coolant temperatures were recorded on magnetic tape for entry into a digital computer. The digital recording system used a sampling rate of 3125 words per second for 125 channels. Since the data were all steady state, 25 readings of each channel were used for smoothing. This smoothing technique, along with the sampling rate, eliminates 60-hertz noise and greatly diminishes any random noise. One report was made for all parameters at a common time. This report was then used in the terminal calculations. Five reports were normally used for one operating condition. The times of these reports could be varied to best represent the steady-state conditions. This reduced the amount of terminal calculations.

Test Procedure

The rocket engine (fig. 4) was installed on a test stand at the Plum Brook Station of the Lewis Research Center. The facility and engine were designed so the coolant flow and coolant pressure could be controlled independently of the operating condition on the hot-gas side. This was achieved by directing the coolant flow to a burnoff system instead of to the injector as is normal for a regenerative system. To set a test point after a chilldown of the engine, first a high coolant flow was established. Then the propellant valves for controlling gaseous hydrogen and liquid oxygen were automatically set to ramp open to establish a given hot-gas side chamber pressure and percent fuel. As these were established, coolant flow and pressure were then controlled to set values for these conditions. Thus, a range of coolant flows and pressures could be run for one hot-gas side operating condition. Table II gives the various running conditions.

CALCULATION PROCEDURE

Experimental Hot-Gas-Side and Coolant-Side Heat-Transfer Coefficients

Hot-gas-side heat-transfer correlations for the injector and thrust chamber used in the present investigation were reported in references 2 and 3. These correlations were obtained from transient tests with an instrumented copper nozzle that had the same internal gas-side geometry as the liquid-cooled nozzle used in the present investigation.

The heat flux q to the five instrumented axial stations was determined from the relation

$$q = h_g(T_{a,w} - T_{g,w}) \tag{1}$$

where the value of the hot-gas-side heat-transfer coefficient h_g was determined from the transient tests reported in references 2 and 3 and from additional unpublished data that resulted in correlations of the form $St^* Pr^{*0.7} = C_g Re_d^{*-0.2}$. The curve of the correlating constant C_g as a function of axial position used is given in figure 5. The gas-side wall temperature $T_{g,w}$ was measured with a specially developed thermocouple previously described. The adiabatic wall temperature $T_{a,w}$ was computed by using the method described in reference 2.

The coolant-side wall temperature was obtained from the relation

$$q = \frac{k}{b}(T_{g,w} - T_{c,w}) \tag{2}$$

where k is the thermal conductivity of the AISI-347 stainless-steel tube wall, b is the tube wall thickness, and $T_{c,w}$ is the coolant-side wall temperature.

The coolant temperature and pressure were measured at each axial station so that the coolant-side heat-transfer coefficient h_c could be obtained from the relation

$$q = h_c(T_{c,w} - T_c) \tag{3}$$

where T_c is the coolant temperature.

Coolant-Side Heat-Transfer Correlations

Several correlation schemes were also used to calculate hot-gas-side wall temperature. This temperature could then be compared directly with the measured value of wall temperature. To perform this calculation, a digital computer program was set up. The input to the computer program used the measured coolant flow, the coolant-inlet pressure, the coolant temperature, and the tube flow area. The required hot-gas-side inputs were h_g and $T_{a,w}$ which were obtained as described previously.

Film-type correlation. -

$$St^* Pr^{*0.6} = 0.023\ Re^{*-0.2}\ \varphi_1\varphi_2 \tag{4}$$

where all the transport properties are introduced at a film reference temperature, where the reference temperature is defined as $T^* = (T_{c,s} + T_{c,w})/2$. The terms φ_1 and φ_2 are correction terms for curvature and entrance effects which are described later, in the section titled Geometric Effects.

Modified Hess and Kunz correlation (ref. 7). -

$$St^* Pr^{*0.6} = 0.0208\ Re^{*-0.2}\left(1 + 0.01452\ \frac{\mu_{c,w}}{\mu_{c,s}}\right)C_L\varphi_1\varphi_2 \tag{5}$$

where the term C_L was added (refs. 8 and 9) to provide a better fit to available experimental data. The term C_L varies nonlinearly as a function of $T_{c,s}$, as shown by the following table:

$T_{c,s}$		C_L
K	°R	
27.8	50	2.0
33.3	60	1.48
38.9	70	1.07
44.4	80	6.87
47.2	85	.85

Taylor correlation (ref. 6). -

$$St_s Pr_s^{0.6} = 0.023\ Re_s^{-0.2}\ (\varphi_1\varphi_2)\left(\frac{T_{c,w}}{T_{c,s}}\right)\exp\left[-\left(0.57 - \frac{1.59}{\sum\frac{\Delta S}{D}}\right)\right] \tag{6}$$

where the subscript s refers to transport properties evaluated at bulk, or static, temperature.

Correlation for supercritical-pressure hydrogen with a new integration technique for transport properties. - The forced-convection heat-transfer coefficients for single-phase fluids flowing in tubes have been correlated by means of dimensionless numbers. These single-phase fluids generally have transport properties that vary moderately with temperature. The equation

$$\frac{h}{\rho V c_p}\left(\frac{c_p \mu}{k}\right)^m = \left(\frac{\rho V d}{\mu}\right)^n C \tag{7}$$

was used for the correlation. The bulk, film, and wall temperatures were used for evaluating the properties c_p, μ, Pr, and ρ. Other investigators have found that a reference temperature or reference enthalpy is best for property evaluation. Equation (7) is unsatisfactory for correlating hydrogen at supercritical pressure because of the large variations in transport properties within the film boundary layer when the film temperature passes through the pseudocritical region. Reference 10 showed that the heat-transfer coefficient for supercritical water was not a unique function of film temperature or of any other single temperature. Since the transport properties for any fluid are unique functions of pressure and temperature, and since the temperature varies across the boundary layer, all properties were evaluated by use of the following equation:

$$\bar{x} = \frac{\int_{T_{c,s}}^{T_{c,w}} x \, dT}{T_{c,w} - T_{c,s}} \tag{8}$$

where x is the property c_p, μ, ρ, or $c_p\mu/k$ at static pressure. Reference 10 used this technique on c_p. The integration technique takes care of the irregular variation of properties in the pseudocritical temperature range, and the same nondimensional numbers used in equation (7) should give satisfactory correlation with $m = 0.6$, $C = 0.023$, and $n = -0.2$ for supercritical-pressure hydrogen in the range of tests covered by these rocket firings.

The integration scheme for introducing transport properties is more complicated, but with the advent of high-speed computers programmed to use Gaussian quadrature numerical integration schemes, the computing time is minimized. Computation takes no longer than with the other coolant-side correlations.

Before any correlation can be accepted, it must be evaluated for its reliability on many sets of experimental data over as large a range of the variables as possible. The handling of transport properties is the unique part of the correlation used in this report. One can readily see that in regions where the transport properties vary in an approximately linear fashion with temperature, this correlation will work as well as any of the older type correlations where a reference temperature is used for evaluating the transport properties. Therefore, this correlation needs to be checked only in regions where the transport properties have large changes with small changes in temperature, as occurs with hydrogen near the pseudocritical temperature

Reference 4, which was an experimental study of a regeneratively cooled hydrogen-fluorine engine, found that a coolant-side heat-transfer correlation of the form $Nu = C\,Re^{0.8}Pr^{0.33}$ gave a satisfactory local correlation, but the C values needed for S/d values of approximately 10 were 0.045 or higher. Transport properties in reference 4 were evaluated at a film temperature. Where integrated transport properties are used in the correlation, the constant C is reduced to 0.028 for run 9 of this reference without an entrance correction factor. The entrance factor used in the present report would be 1.36 for an S/d of 10; therefore, C is really 0.021. The coolant temperature for the hydrogen was 44.4 K (80° R) at this location. The inlet static pressure for this S/d was 0.951 meganewtons per square meter absolute (138 psia), which is below the critical pressure for hydrogen. But in this region, the transport properties are still varying with temperature.

Two runs of reference 5, which flowed cryogenic hydrogen in electrically heated tubes, were also used as a test for this correlation.

Table III summarizes the results of the present investigation and compares the experimental heat-transfer coefficient (h) with the coefficients calculated by the Schacht

and Quentmeyer correlation (h_{SQ}) of the present investigation, the Hess and Kunz correlation (h_{HK}) from reference 7, the McCarthy and Wolf correlation (h_{MW}) from reference 13, and the film correlation (h*) from reference 5. On the basis of this comparison, the new method of evaluating properties seemed satisfactory. The main advantage of this technique is that the correlation does not have to be altered in going from the subcritical to the supercritical temperature regime (i. e., needs no altering of the constants or exponents).

Geometric Effects

Curvature effects. - The coolant-side correlations discussed so far are valid only for straight pipes. In curved pipes, a secondary flow exists, because that part of the flow near the flow axis is acted upon by a larger centrifugal force than the slower flow near the inner wall. Reference 14 indicates that the resistance coefficient λ for turbulent flow in a curved pipe can be represented by

$$\varphi_1 = \frac{\lambda}{\lambda_o} = \left[\mathrm{Re}\left(\frac{R}{r}\right)^2\right]^{0.05} \quad \text{for} \quad \mathrm{Re}\left(\frac{R}{r}\right)^2 > 6 \tag{9}$$

where λ_o is the resistance coefficient for a straight pipe, R is the cross-sectional radius, r is the radius of curvature, and Re is the Reynolds number. Reference 15 found the curvature effect required a finite distance (approx. 15 diameters) in which to develop, and a persistence effect that required 14 or more diameters of the curve to dissipate. This study also found lower enhancement factors with low bulk temperatures. This factor, however, may be offset by the enhancement due to the acceleration effects caused by the converging tube geometry as the throat or curvature section is approached.

The study also showed that reverse curvature (where the more dense fluid is directed away from the surface to be cooled by centrifugal force) did not always detract from heat transfer but approached that of a straight tube. Also, in tubes that had a curvature followed by a reverse curve (such as the case of a rocket thrust chamber tube), the heat-transfer enhancement persisted beyond the first curve and was followed by a transition length. Therefore, depending on the geometric configuration, the reverse-curve section could have heat transfer either greater than, equal to, or less than the straight tube.

In the present tests, coolant-side heat-transfer coefficients were obtained at five axial stations, three of which were in the curvature, reverse-curvature region. Five locations are not enough to provide the detailed information needed for complete description of the curvature, reverse-curvature situation. An enhancement factor was, there-

fore, constructed with the use of available station data. The magnitude and distribution of this enhancement factor is illustrated in figure 6. A value of 1.0 was assigned at the tangent point where the curvature begins. From this point, the factor was allowed to increase to a maximum of 1.52 approximately 25 diameters downstream of the tangent point (which is the value predicted in ref. 14 by the Ito equation for this geometry). The enhancement factor was then reduced to a value of 1.0 at the tangent point at the end of the reverse-curvature region. The curvature correction factor was used in the digital computer program to provide a heat-transfer enhancement in the curvature region.

Entrance effects. - Boelter, Young, and Iversen (ref. 16) reported the results of experiments with air flowing through a steam-heated tube in which the steam jacket was sectioned in such a way that the local heat-transfer rate at each section could be determined from a measurement of the condensate rate. A curve fit of the entrance data for a 90° entrance angle gave the equation

$$\varphi_2 = \frac{2.88}{\left(\frac{S}{d}\right)^{0.325}} \tag{10}$$

The entrance coefficient φ_2 is not allowed to be less than 1. This equation was used to provide the entrance heat-transfer enhancement factor in the digital-computer program for tube-wall-temperature evaluation. Other investigators, including reference 16, have used an entrance factor of the form $\varphi_2 = [1 + F(d/S)]$. Taylor (ref. 6) suggests a value of $F = 5.0$ for a 90° entrance angle, which is normally used for an overall effect instead of a local effect.

Asymmetric heating and roughness effects. - Experiments with straight tubes have shown asymmetric heating to have only a minor effect on heat transfer. However, the effect of asymmetric heating in curved tubes could be significant. Inasmuch as no data exist for the curved-tube portion of the engine, no correction for asymmetric heating was used.

Rough tube walls have little effect on laminar-flow heat transfer, but the effect can be great for turbulent flow. If the surface roughness is as thick as the laminar sublayer, the roughness breaks up the sublayer and increases the wall shear stress. If the surface is sufficiently rough, the shear forces are transmitted to the wall in the form of pressure drag on the irregularities, and the friction coefficient becomes practically independent of Reynolds number. In the present work, no roughness effects were accounted for in the heat transfer.

Friction Pressure Loss Calculations

Pressure losses include the sum of momentum and frictional losses. Frictional pressure drop is normally computed from an equation of the form $\Delta P = fS\rho V^2/2gd$. The friction factors used in the pressure-drop calculations were

$$f = \frac{64}{Re^*}\left(\frac{\lambda}{\lambda_o}\right) \quad \text{for} \quad Re^* < 2.2\times10^3 \tag{11}$$

$$f = 4\left(0.0014 + \frac{0.125}{Re^{*0.32}}\right)\left(\frac{\lambda}{\lambda_o}\right) \quad \text{for} \quad 2.2\times10^3 < Re^* < 1\times10^4 \tag{12}$$

$$f = 0.078\ Re^{*-0.1021}\left(\frac{\lambda}{\lambda_o}\right) \quad \text{for} \quad Re^* > 1\times10^4 \tag{13}$$

where

$$Re^* = \frac{\rho^* V d_h}{\mu^*}$$

$$\rho^* = f(T^*, P_s) = \frac{\int_{T_{c,s}}^{T_{c,w}} \rho\, dT}{T_{c,w} - T_{c,s}}$$

and λ/λ_o is defined in the Curvature effects section. In Taylor's correlation, a Reynolds number based on transport properties introduced at wall conditions is used. In the Hess and Kunz and the film correlations, a Reynolds number based on transport properties evaluated at static conditions is used.

For Reynolds numbers greater than 1×10^4, the equation $f = 0.078\ Re^{*-0.1021}$ was used, which corresponds roughly to having a surface irregularity of 1.905 micrometers rms (75 μin. rms). Profilometer measurements taken on engine coolant tube specimens revealed readings of approximately 1.626 micrometers rms (64 μin. rms) in the curved region that forms the nozzle throat.

DISCUSSION OF RESULTS

Table II gives a tabulation of the various running conditions. It should be noted that with the exception of thrust chamber 5, all thrust chambers were identical; thrust chamber 5 had a wall thickness of 0.0254 centimeter (0.010 in.).

Runs 83 and 91 had approximately the same operating conditions on both the hot-gas side and the coolant side but were obtained from two different engines. Figure 7 is a plot of the hot-gas wall temperature $T_{g,w}$ as a function of axial position X for these two runs. The calculated values in this figure are for run 91. The spread of the experimental data for both tubes for both engines is shown in this plot. Appendix B gives the results of a study of two-dimensional instrumentation effects. Since the corrections from one-dimensional to two-dimensional effects are small, one-dimensional predicted values are compared with measured thermocouple readings in all results that follow. The hot-gas wall-temperature values predicted by the three coolant-side correlations that have more or less industry-wide recognition are also shown in figure 7. The film-type coolant-side correlation (eq. (4)), where all transport properties are inserted at a film temperature, is quite unsatisfactory in the regions upstream and downstream of the throat. The Taylor coolant-side correlation (eq. (6)) gives a fairly reasonable representation of the hot-gas wall temperature in the entrance region and up to the throat. It underpredicts the throat region and it overpredicts the chamber region close to the throat. The modified Hess and Kunz coolant-side correlation (eq. (5)) does a good job of predicting the hot-gas-side wall temperatures in all regions except the throat. In all of these correlations, an Ito type curvature correction was used, along with an entrance factor of $[1 + (5d/S)]$.

Figure 8 is a plot of the hot-gas wall temperature as a function of axial location as predicted by the use of the coolant-side correlation (eq. (7)) where all transport properties are introduced by an integration method (eq. (8)) and with the values of $m = 0.6$, $C = 0.023$, and $n = -0.2$. In this correlation, the curvature correction of figure 6 and the entrance correction of equation (10) were used. This correlation predicts the hot-gas wall temperature fairly well in all regions except for a region right at the throat, where it underpredicts the hot-gas wall temperature. This correlation, with the evaluation of properties by an integration technique, is recommended. It needs no additional corrections in the regions of low bulk temperature, and standard entrance corrections that are used for other fluids seem to give sufficient correction in the entrance regions.

A plot of the experimental coolant static pressure as a function of axial location for both tubes for run 91 is presented in figure 9. The predictions for the static pressure by the film correlation and the modified Hess and Kunz correlations use the friction factor of equation (12), with properties introduced at the static pressure and temperature. In the Taylor correlation, a correction term, $(T_{c,s}/T_{c,w})^{0.5}$, is multiplied by equa-

tion (12), and all properties are introduced at the coolant wall temperature and static pressure. All three of these correlations do a good job of predicting the pressure drop in the nozzle region up to the throat, but they underpredict the pressure drop in the chamber region. The coolant correlation with all properties inserted with the integration scheme (eq. (8)) and with a friction factor computed by the use of equation (13) does a better job of predicting the pressure drop in the chamber region.

Figure 10 presents a plot of the experimental coolant temperature as a function of axial location for run 91. All the coolant-side correlations underpredict the coolant temperature rise, with the film-type correlation doing the worst job.

In the preceding computations, the heat flow rates q as functions of axial location X were all obtained from the hot-gas wall temperature and the hot-gas-side heat-transfer correlations from references 2 and 3. These correlations use the correlation constant C_g as a function of axial location X from figure 5. There is always some uncertainty in this constant. Figure 11 shows a plot of the hot-gas wall temperature as a function of axial location for run 91, where C_g has been increased by 15 percent. This figure also shows the effect of decreasing the coolant-side correlation constant C_c by 15 percent. The coolant-side correlation with properties inserted by the integration scheme was used for this figure. The hot-gas wall temperatures are increased by 111.1 K (200° R) or less by this increase in C_g or decrease in C_c. The temperatures are all higher than the experimentally measured values. This plot shows the sensitivity of the hot-gas wall temperature to changes in C_g or C_c and tends to make one believe that both the hot-gas-side correlation and the new coolant-side correlation are adequate for evaluating the present design.

To show the sensitivity of the design to inlet pressure and temperature, first the inlet pressure of run 91 was varied, and then the inlet temperature. Figure 12 shows a plot of the calculated hot-gas wall temperature for inlet pressures of 4.88 and 7.58 meganewtons per square meter absolute (708 and 1100 psia), and for inlet temperatures of 28.19 and 55.56 K (50.74° and 100° R). These changes in inlet pressure and inlet temperature both reduce the hot-gas wall temperature for this design. One must remember that these effects come about for a given tube geometry and were, therefore, not optimized for these inlet conditions.

Figures 13 to 16 are plots of the predicted and experimental values of the hot-gas-side wall temperature as a function of axial location for the other running conditions of table II (runs 44, 79, 92, and 94, respectively). The maximum error is an overprediction of 211.1 K (380° R) in the chamber region for run 92. The maximum underprediction is 166.7 K (300° R) in the chamber region of run 79, but the data spread at this station is also 166.7 K (300° R). The maximum error in the throat region for these runs was 83.3 K (150° R).

Figures 17 to 21 are plots of the predicted and measured static pressures as functions of axial location for runs 44, 79, 83, 92, and 94. The maximum error in predict-

ing the pressure is an overprediction of 0.689 kilonewtons per square meter (100 psi), which corresponds to an underprediction of the pressure drop.

Figures 22 to 26 are plots of the predicted and measured coolant temperatures as functions of axial location for runs 44, 79, 83, 92, and 94. The coolant temperature rise in this type of design is small, because all the propellant flow for a nuclear thrust chamber goes through the coolant passage. The predictions of the temperature rise through the tubes are generally low, but are considered adequate for designs of this type.

CONCLUDING REMARKS

The new correlation, of the form $StPr^{0.6} = 0.023\,Re^{-0.2}$, where all transport properties are inserted by an integration technique, does a reasonable job of predicting the coolant-side heat-transfer coefficients for hydrogen near the pseudocritical temperature region in the present work. This correlation should be tried over a greater range of the variables than was encountered in the present work and should also be tried for other fluids.

A small study of the cooling characteristics of liquid hydrogen was made with the use of the new integration technique. This study is presented in appendix C. The heat-transfer coefficient for liquid hydrogen increases with bulk temperature for a given coolant-side wall temperature in the region of coolant static pressures at or near 3.447 meganewtons per square meter absolute (500 psia). The heat flow rate reaches a maximum at an optimum bulk temperature for a given coolant-side wall temperature. If one considers Mach number to be a measure of coolant pressure drop, the new correlation shows that a designer should stay at the lowest bulk temperature possible or a compromise must be made between maximum heat-transfer coefficient and heat flow rate and minimum pressure drop. The preceding remarks are all limited to coolant static pressures near 3.447 meganewtons per square meter absolute (500 psia). These studies should be carried out over other pressure ranges. Great gains in the use of the coolant capabilities of liquid hydrogen should be possible by optimization based on such studies.

SUMMARY OF RESULTS

An experimental investigation was conducted at the NASA Lewis Research Center to determine the coolant-side heat-transfer rates in a liquid-hydrogen-cooled, rocket thrust chamber, where the coolant was near the pseudocritical temperature region. Local measurements of the hot-gas-side wall temperatures, coolant temperatures, and coolant pressures were made at five axial stations on two coolant tubes. The test data

were compared with calculated data obtained from several leading existing correlations and a new technique for data correlation. The following results were obtained:

1. Correlations of the form $StPr^{0.6} = 0.023\ Re^{-0.2}$ (where St is Stanton number, Pr is Prandtl number, and Re is Reynolds number) with all coolant properties introduced at a reference or film temperature do an inadequate job of correlating the data in the present work.

2. The modified, coolant-side correlation of Hess and Kunz and the coolant-side correlation of Taylor both correlate the test data of the present investigation reasonably well, with some limitation.

3. A correlation of the form $StPr^{0.6} = 0.023\ Re^{-0.2}$ with all properties introduced by an integration technique gives a reasonable correlation of the present test data. This technique has the advantage that no corrections are needed for low bulk temperatures, and standard entrance corrections can be used.

4. Ito's curvature correction gives about the right magnitude for the curvature enhancement term in the throat region.

5. Standard friction factors with roughness taken into account predict the pressure drops reasonably well when they are used with the coolant correlation that introduces transport properties evaluated by the integration technique.

6. The use of microminiature thermocouples provided good local measurements of hot-gas wall temperatures, but the life of these thermocouples was short.

Lewis Research Center,
National Aeronautics and Space Administration,
Cleveland, Ohio, December 5, 1972,
503-35.

APPENDIX A

SYMBOLS

A	cross-sectional area
a	sonic velocity
b	tube wall thickness
C	correlation constant
C_L	coolant low-bulk temperature correction
c_p	specific heat
d	diameter
F	entrance-factor constant
f	friction factor
g	gravitational constant
h	heat-transfer coefficient
h'	coolant-channel height perpendicular to flow
k	thermal conductivity
L^*	characteristic length of thrust chamber, V/A_{th}
M	Mach number
m	Prandtl number exponent
n	Reynolds number exponent
Nu	Nusselt number, hd/k
P	pressure
Pr	Prandtl number, $c_p\mu/k$
q	heat flow rate
R	cross-sectional radius of coolant channel
r	radius of curvature
Re	Reynolds number, $\rho Vd/\mu$
S	distance along tube from coolant-inlet manifold (see fig. 1)
St	Stanton number, $h/\rho Vc_p$
T	temperature

V	velocity
v	combustion chamber volume
$\dot{W}$	coolant weight flow
w	chord width of channel
X	axial location relative to throat (negative values upstream of throat; positive values downstream of throat)
x	transport property (ρ, c_p, μ, or k)
$\bar{x}$	transport property defined by eq. (8)
λ	resistance coefficient for turbulent flow in a curved pipe
λ_o	resistance coefficient for turbulent flow in a straight pipe
μ	viscosity
ρ	density
φ_1	curvature correction coefficient, λ/λ_o
φ_2	entrance correction coefficient

Subscripts:

a	adiabatic
c	coolant
d	diameter
g	hot-gas side
h	hydraulic
HK	Hess and Kunz
in	inlet
MW	McCarthy and Wolf
o	straight tube
SQ	Schacht and Quentmeyer
s	bulk, or static
th	throat
u	interface between the nickel plating and the AISI-347 stainless-steel wall
w	wall

Superscript:

*	reference or film

APPENDIX B

TWO-DIMENSIONAL INSTRUMENTATION EFFECTS

The hot-gas-side wall thermocouples used in these tests were protected by a 0.0127- to 0.0254-centimeter (0.005- to 0.010-in.) layer of nickel that was electroplated over the 0.00127- to 0.00254-centimeter (0.0005- to 0.001-in.), Platinel-7674-alloy, quartz-insulated, thermocouple wire. Since nickel has a higher conductivity than the AISI-347 stainless-steel tube wall, the readings of the thermocouples should have been corrected in order to compare directly with the hot-gas wall temperatures predicted by the various correlations, where only one-dimensional heat flow was taken into account and only AISI-347 stainless-steel material was used. In order to show the magnitude of these corrections, calculations were carried out for a typical run (run 91) for the throat and chamber stations. Table IV summarizes these calculations.

For example, at the throat, the measured value would have been 659.4 K (1187° R) if the thermocouple had been covered with a 0.0254-centimeter (0.010-in.-) layer of nickel. The predicted value from the correlation that used one-dimensional heat flow and only AISI-347 stainless steel was 700.5 K (1261° R). In the chamber, these two values would have been 742.2 K (1336° R) and 745.5 K (1342° R). However, the true values of the hot-gas wall temperature at any spot at the throat and chamber not affected by instrumentation would have been 692.2 K (1246° R) and 766.7 K (1380° R), respectively. Since the corrections from one-dimensional to two-dimensional effects are small and the corrections from the 0.0254-centimeter (0.010-in.) nickel coating to no nickel coating are also small, no further tests were run, and using one-dimensional predicted values to compare with the measured thermocouple readings was considered a good comparison.

APPENDIX C

DESIGN SIGNIFICANCE OF THE CORRELATION THAT USES THE INTEGRATION TECHNIQUE FOR PROPERTY EVALUATION

In order to optimize a coolant design with the use of the new correlating technique, one should examine the parameters h and q over a range of coolant temperatures and coolant-side wall temperatures. This is shown graphically herein for one coolant pressure. Pressure drop is also considered.

The coolant side correlation $StPr^{0.6} = C\ Re^{-0.2}$ can be rewritten as

$$\frac{h_c d^{0.2}}{0.023\left(\frac{\dot{W}}{A}\right)^{0.8}} = \frac{\bar{c}_p \bar{\mu}^{0.2}}{\overline{Pr}^{0.6}}\left(\frac{\bar{\rho}}{\rho_{c,s}}\right)^{0.8}$$

where all properties are introduced by the use of the integration technique

$$\bar{x} = \frac{\int_{T_{c,s}}^{T_{c,w}} x\, dT}{T_{c,w} - T_{c,s}}$$

where x is the property c_p, μ, ρ, or Pr.

Figure 27 is a plot of $h_c d^{0.2}/0.023(\dot{W}/A)^{0.8}$ as a function of the static, or bulk, temperature $T_{c,s}$ for various coolant-side wall temperatures $T_{c,w}$. The static pressure was held at 3.447 meganewtons per square meter absolute (500 psia). This plot shows that the coolant-side heat-transfer coefficient h_c for a given coolant flow and cross-sectional area increases with coolant temperature for a given coolant wall temperature. However, if the preceding equation is reworked in terms of the heat flow rate q, the equation becomes

$$\frac{q d^{0.2}}{0.023\left(\frac{\dot{W}}{A}\right)^{0.8}} = \frac{\bar{c}_p \bar{\mu}^{0.2}}{\overline{Pr}^{0.6}}\left(\frac{\bar{\rho}}{\rho_{c,s}}\right)^{0.8}(T_{c,w} - T_{c,s})$$

Then the heat flow rate q that the coolant picks up for a given flow and cross-sectional area reaches a maximum at some bulk temperature for a given $T_{c,w}$, as shown in fig-

ure 28. The bumps in these plots are caused by property variations around the pseudo-critical temperature point and are showing up probably only because of the integration technique chosen or because of the technique used for obtaining the properties in this region.

So far, only the heat-transfer parameters of the coolant have been considered. If one considers the pressure drop, which is another important parameter for any design, one can also introduce the Mach number in the parameter $\dot{W}/A$ by the following manipulation:

$$\frac{\dot{W}}{A} = \rho_{c,\,s} V = \frac{\rho_{c,\,s} Va}{a} = \rho_{c,\,s} Ma$$

Figure 29 shows a plot of the equation

$$\frac{qd^{0.2}}{0.023\ M^{0.8}} = \frac{\bar{c}_p \bar{\mu}^{0.2}}{\overline{Pr}^{0.6}} \left(\frac{\bar{\rho}}{\rho_{c,\,s}} \right)^{0.8} (T_{c,\,w} - T_{c,\,s})(\rho_{c,\,s} a)^{0.8}$$

This plot shows that q for a given Mach number increases with decreasing $T_{c,\,s}$ for a given coolant wall temperature $T_{c,\,w}$.

It can also be seen from this equation that q increases with increasing Mach number; however, pressure drop also increases with increasing Mach number. Thus, if pressure drop is an important consideration for a given design, a compromise must be made between maximizing h and q and minimizing pressure drop.

These plots are all for a coolant pressure of 3.447 meganewtons per square meter absolute (500 psia). A designer can make similar plots to cover the range of pressures needed and then use the plots to gain an insight to the optimization of a particular design.

REFERENCES

1. Hall, W. B.; Jackson, J. D.; and Watson, A.: A Review of Forced Convection Heat Transfer to Fluids at Supercritical Pressures. Presented at the Inst. Mech. Eng. Symposium on Heat Transfer and Fluid Dynamics of Near Critical Fluids, Bristol, England, Mar. 27-29, 1968.

2. Schacht, Ralph L.; Quentmeyer, Richard J.; and Jones, William L.: Experimental Investigation of Hot-Gas Side Heat-Transfer Rates for a Hydrogen-Oxygen Rocket. NASA TN D-2832, 1965.

3. Schacht, Ralph L.; and Quentmeyer, Richard J.: Axial and Circumferential Variations of Hot-Gas-Side Heat-Transfer Rates in a Hydrogen-Oxygen Rocket. NASA TN D-6396, 1971.

4. Curren, Arthur N.; Price, Harold G., Jr.; Krueger, Roger C.; and Manning, Frank L. C.: Experimental Heat-Transfer Study of a Regeneratively Cooled Hydrogen-Fluorine Rocket Engine at Low Chamber Pressure. NASA TN D-4178, 1967.

5. Hendricks, Robert C.; Graham, Robert W.; Hsu, Yih Y.; and Friedman, Robert: Experimental Heat-Transfer Results for Cryogenic Hydrogen Flowing in Tubes at Subcritical and Supercritical Pressures to 800 Pounds per Square Inch Absolute. NASA TN D-3095, 1966.

6. Taylor, Maynard F.: A Method of Predicting Heat Transfer Coefficients in the Cooling Passages of NERVA and Phoebus-2 Rocket Nozzles. NASA TM X-52437, 1968.

7. Hess, H. L.; and Kunz, H. R.: A Study of Forced Convection Heat Transfer in Supercritical Hydrogen. J. Heat Transfer, vol. 87, no. 1, Feb. 1965, pp. 41-48.

8. Anon.: Heat Transfer to Cryogenic Hydrogen Flowing Turbulently in Straight and Curved Tubes at High Heat Fluxes. NASA CR-678, 1967.

9. Anon.: Design Equation Analysis for Heat Transfer to Cryogenic Hydrogen at Pressures from 600 to 1500 psia and Wall-to-Bulk Temperature Ratios to 20. Rep. RN-S-0274, Aerojet-General Corp. (NASA CR-87511), June 1966.

10. Swenson, H. S.; Carver, J. R.; and Kakarala, C. R.: Heat Transfer to Supercritical Water in Smooth-Bore Tubes. Paper 65-WA/HT-25, ASME, Nov. 1965.

11. Deissler, R. G.: Heat Transfer and Fluid Friction for Fully Developed Turbulent Flow of Air and Supercritical Water with Variable Fluid Properties. ASME Trans., vol. 76, no. 1, Jan. 1954, pp. 73-85.

12. Huff, Ronald G.: A Thermocouple Technique for Measuring Hot-Gas-Side Wall Temperatures in Rocket Engines. NASA TN D-5291, 1969.

13. McCarthy, J. R.; and Wolf, H.: The Heat Transfer Characteristics of Gaseous Hydrogen and Helium. Res. Rep. 60-12, Rocketdyne, North American Aviation, Inc. (AD-256802), Dec. 1960.

14. Itō, H.: Friction Factors in Turbulent Flow in Curved Pipes. J. Basic Eng., vol. 81, no. 2, June 1959, pp. 123-134.

15. McCarthy, J. R.: Investigation of Cooling Problems at High Chamber Pressures. Rep. R-6529, Rocketdyne Div., North American Aviation, Inc. (NASA CR-78634), Sept. 15, 1966.

16. Boelter, L. M. K.; Young, G.; and Iversen, H. W.: An Investigation of Aircraft Heaters. XXVII - Distribution of Heat-Transfer Rate in the Entrance Section of a Circular Tube. NACA TN 1451, 1948.

TABLE I. - GEOMETRIC DESIGN DETAILS OF THRUST CHAMBER

AND COOLANT PASSAGES

Design axial station	Axial location relative to throat, X (a)		Coolant-channel height perpendicular to flow, h' (see fig. 1)		Coolant-channel chord width, w (see fig. 1)		Thrust-chamber diameter	
	cm	in.	cm	in.	cm	in.	cm	in.
1	26.807	10.558	0.457	0.180	0.564	0.222	26.632	10.485
[b]2	20.386	8.026	.442	.174	.490	.193	23.178	9.125
3	12.685	4.994	.406	.160	.401	.158	19.050	7.500
[b]4	3.175	1.250	.330	.130	.292	.115	13.952	5.493
5 (Tangent point)	1.643	.647	.323	.127	.277	.109	13.132	5.170
6	.820	.323	.320	.126	.269	.106	12.807	5.042
[b]7 (Throat)	0	0	.318	.125	.267	.105	12.700	5.000
8	-1.643	-.647	.322	.127	.277	.109	13.132	5.170
9 (Tangent point)	-3.175	-1.250	.356	.140	.302	.119	14.402	5.670
[b]10	-5.398	-2.125	.424	.167	.358	.141	16.967	6.680
11 (Tangent point)	-7.605	-2.994	.485	.191	.411	.162	19.530	7.689
12	-12.220	-4.811	.572	.225	.505	.199	23.833	9.383
13	-17.137	-6.747	.622	.245	.561	.221	26.469	10.421
[b]14 (Tangent point)	-22.21	-8.744	.638	.251	.579	.228	27.356	10.77
15	-29.528	-11.625	.665	.262	.579	.228	27.356	10.77
16	-35.278	-13.889	.688	.271	.579	.228	27.356	10.77

[a]Positive values denote locations downstream of throat; negative values denote locations upstream of throat.

[b]Axial locations of instrumentation stations.

TABLE II. - OPERATING CONDITIONS FOR TEST RUNS

Run	Chamber pressure		Oxidant-to-fuel ratio	Hydrogen content, percent	Coolant weight flow		Coolant inlet pressure		Coolant inlet temperature		Tube wall thickness		Thrust chamber
	MN/m^2 abs	psia			kg/sec	lb/sec	MN/m^2 abs	psia	K	^oR	cm	in.	
44	2.088	302.8	6.310	13.68	4.345	9.58	4.238	614.6	27.6	49.7	0.0254	0.010	5
79	2.108	305.8	5.579	15.20	5.384	11.87	4.954	718.5	29.2	52.5	.03048	.012	9
83	2.115	306.7	5.540	15.29	7.058	15.56	5.051	732.6	26.8	48.3	↓	↓	9
91	2.077	301.3	5.502	15.38	7.072	15.59	4.881	708.0	28.2	50.7			12
92	2.070	300.2	5.506	15.37	9.866	21.75	6.337	919.1	30.9	55.7			12
94	3.112	451.2	5.510	15.36	9.902	21.83	6.948	1007.7	30.9	55.7	↓	↓	12

TABLE III. - COMPARISONS OF RATIOS OF MEASURED HEAT-TRANSFER COEFFICIENTS TO PREDICTED HEAT-TRANSFER COEFFICIENTS FOR VARIOUS CORRELATIONS

Run	Length-to-diameter ratio, S/d	Coolant static temperature, $T_{c,s}$		Coolant static pressure, $P_{c,s}$		Ratio of measured heat-transfer coefficient to predicted heat-transfer coefficient				Entrance correction coefficient, φ_2 (see eq. (10))
		K	^{o}R	MN/m^2 abs	psia	h/h_{HK}	h/h_{MW}	h/h^*	h/h_{SQ}	
34 to 273	7.5	30.4	54.7	2.815	408.3	3.54	1.70	3.92	2.053	1.5
	40	40.5	72.9	2.777	402.8	1.16	.69	1.72	1.132	1
57 to 881	7.5	34.9	62.8	4.861	705.1	1.69	1.47	2.27	1.46	1.5
	25	47.0	84.6	4.848	703.2	1.09	.93	1.73	1.135	1.01
	46	61.3	110.4	4.818	698.8	.90	.95	1.20	.906	1

TABLE IV. - TWO-DIMENSIONAL INSTRUMENTATION EFFECTS

Design axial station	Nickel plating, cm (in.)	Hot-gas-side wall temperature, $T_{g,w}$		Interface temperature between wall and plating, $T_{u,w}$	
		K	^{o}R	K	^{o}R
Temperatures from two-dimensional calculations					
7 (throat)	None	692.2	1246	692.2	1246
	0.0254 (0.010)	736.7	1326	659.4	1187
14 (chamber)	None	766.7	1380	766.7	1380
	0.0254 (0.010)	776.7	1398	742.2	1336
Temperatures from one-dimensional calculations					
7 (throat)	None	700.5	1261	700.5	1261
	0.0254 (0.010)	750.6	1351	687.8	1238
14 (chamber)	None	745.5	1342	745.5	1342
	0.0254 (0.010)	768.8	1384	743.3	1338

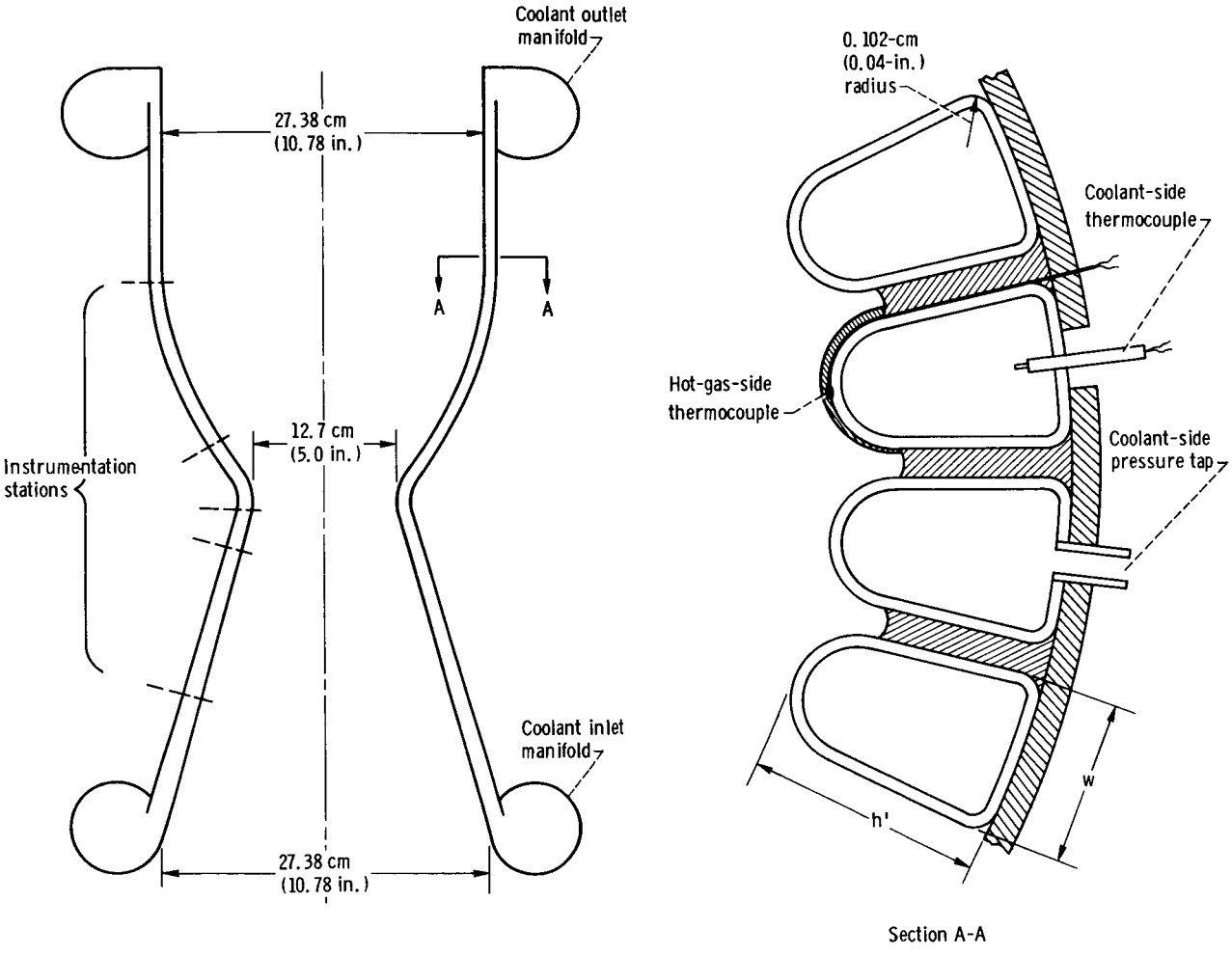

Figure 1. - Liquid-hydrogen-cooled thrust chamber.

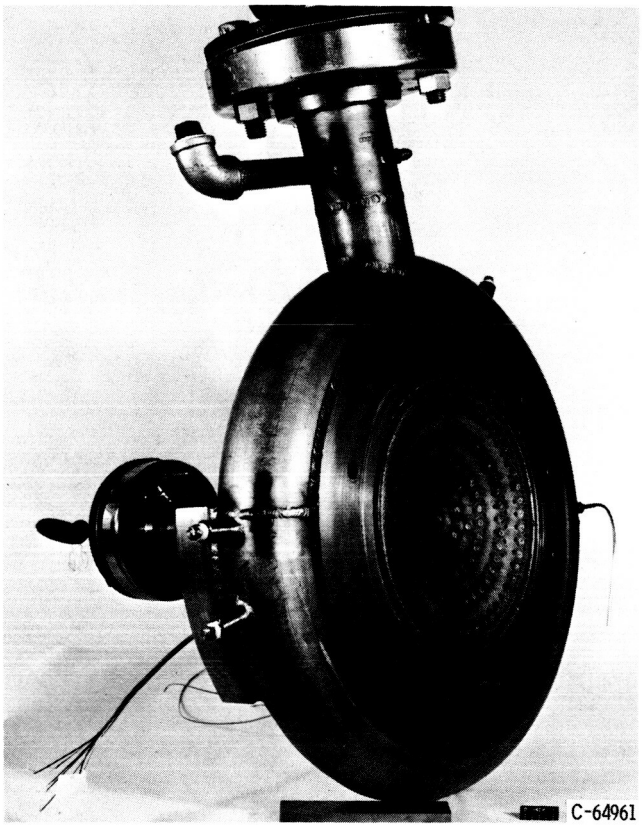

Figure 2. - Coaxial, 234-element injector.

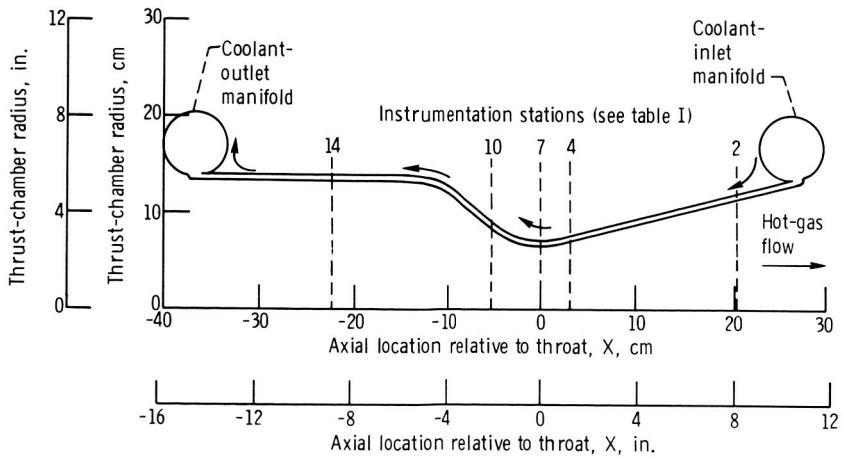

Figure 3. - Axial locations of instrumentation stations relative to throat of thrust chamber.

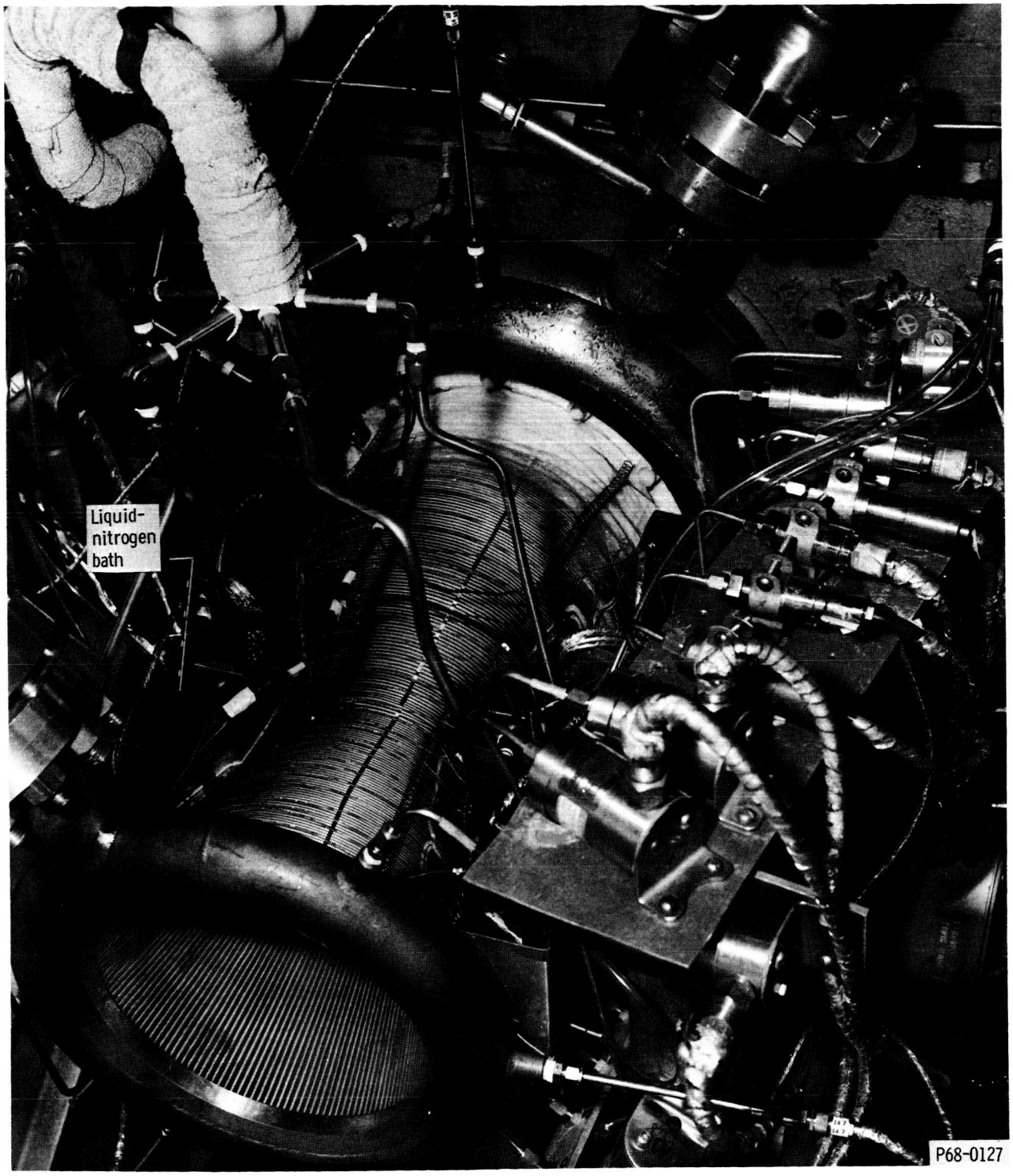

(a) Top view.

Figure 4. - Rocket engine installed on test stand.

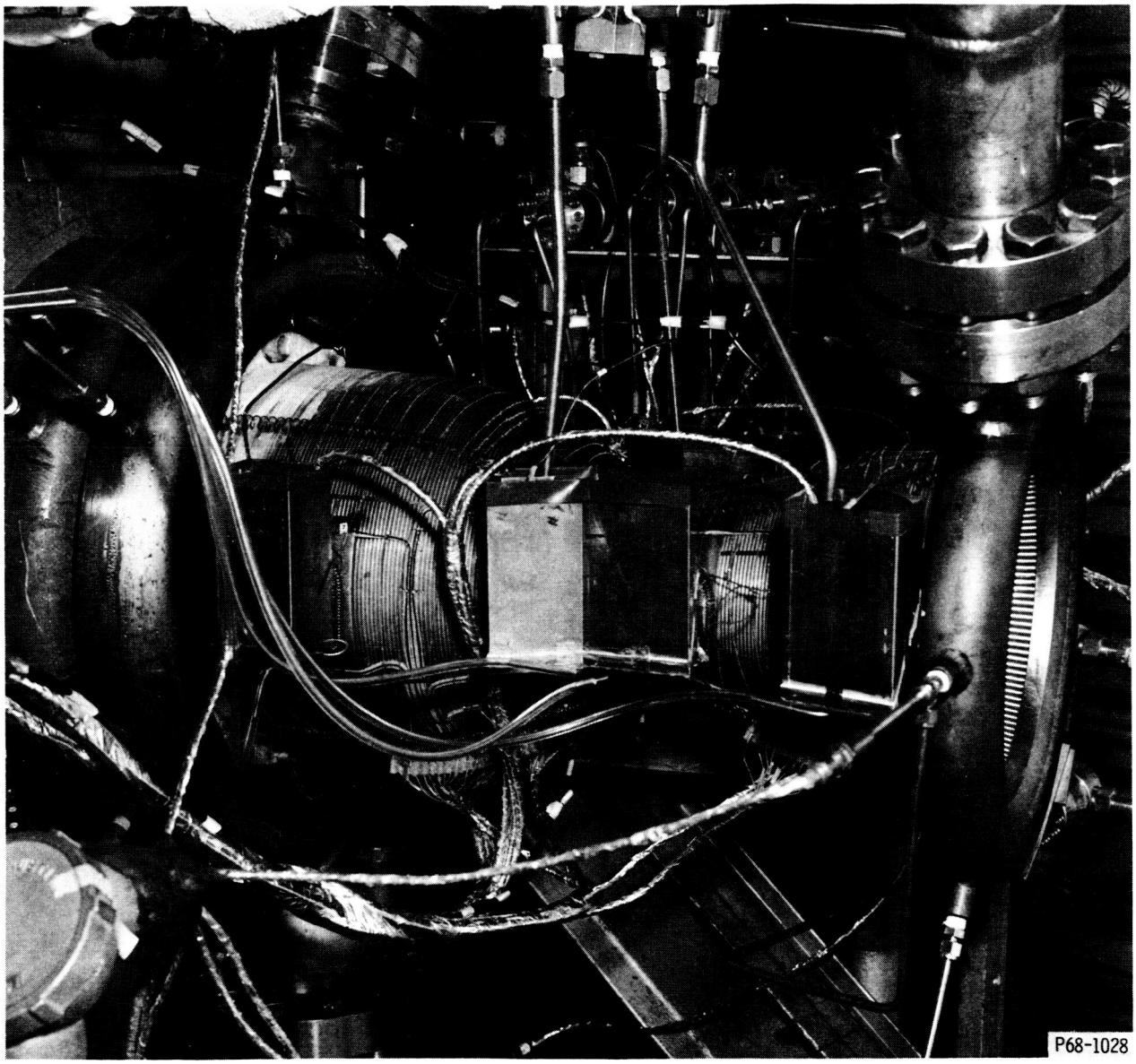

(b) Side view.

Figure 4. - Concluded.

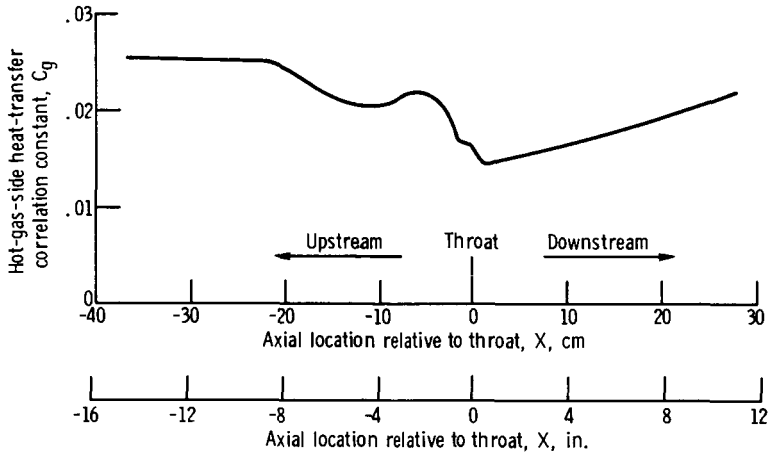

Figure 5. - Hot-gas-side heat-transfer correlation constant as a function of axial location for a correlation of the form $St\ Pr^{0.7} = C_g\ Re^{-0.2}$.

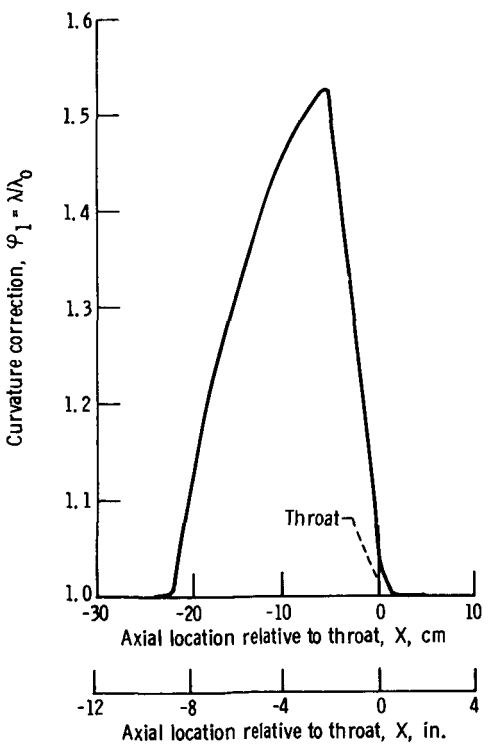

Figure 6. - Curvature correction as a function of axial location. Data from run 91.

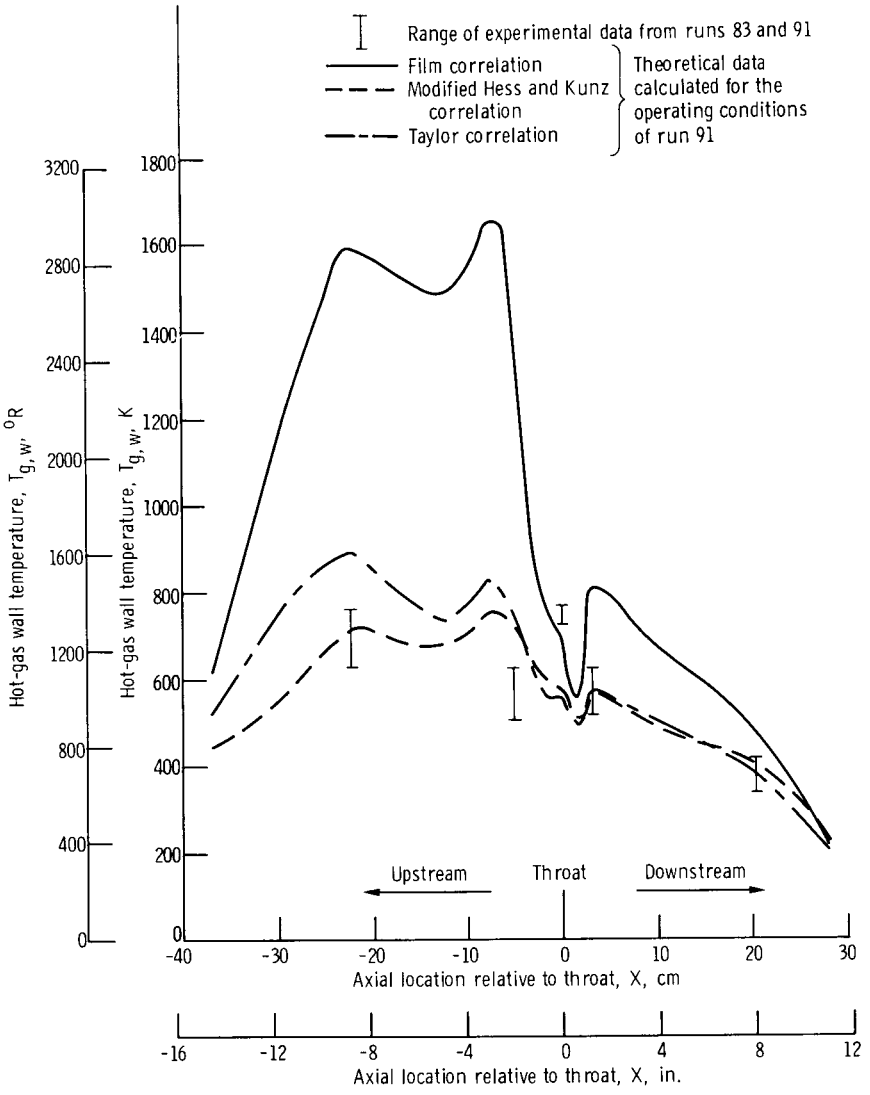

Figure 7. - Experimental and theoretical hot-gas wall temperatures as functions of axial locations for various coolant correlations.

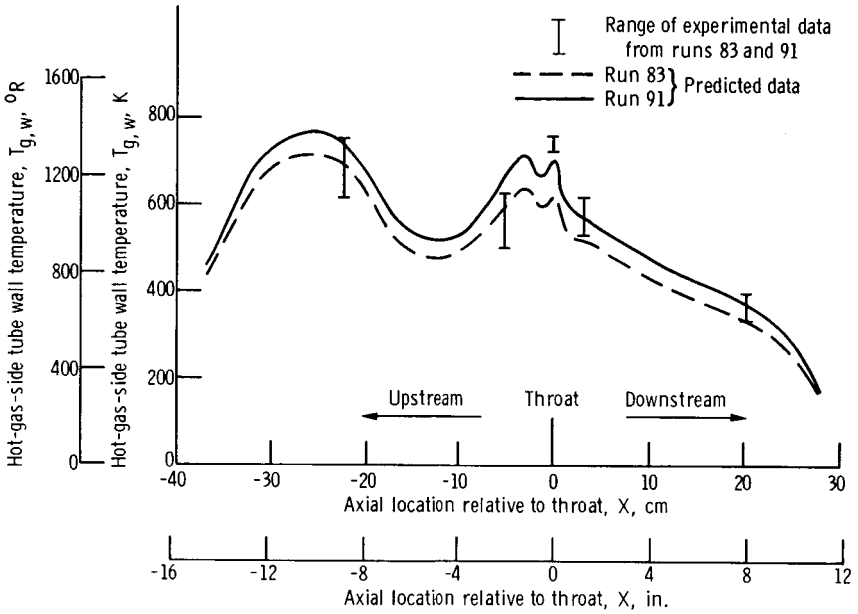

Figure 8. - Hot-gas-side wall temperature, as function of axial location, predicted by correlation with properties evaluated by integration technique.

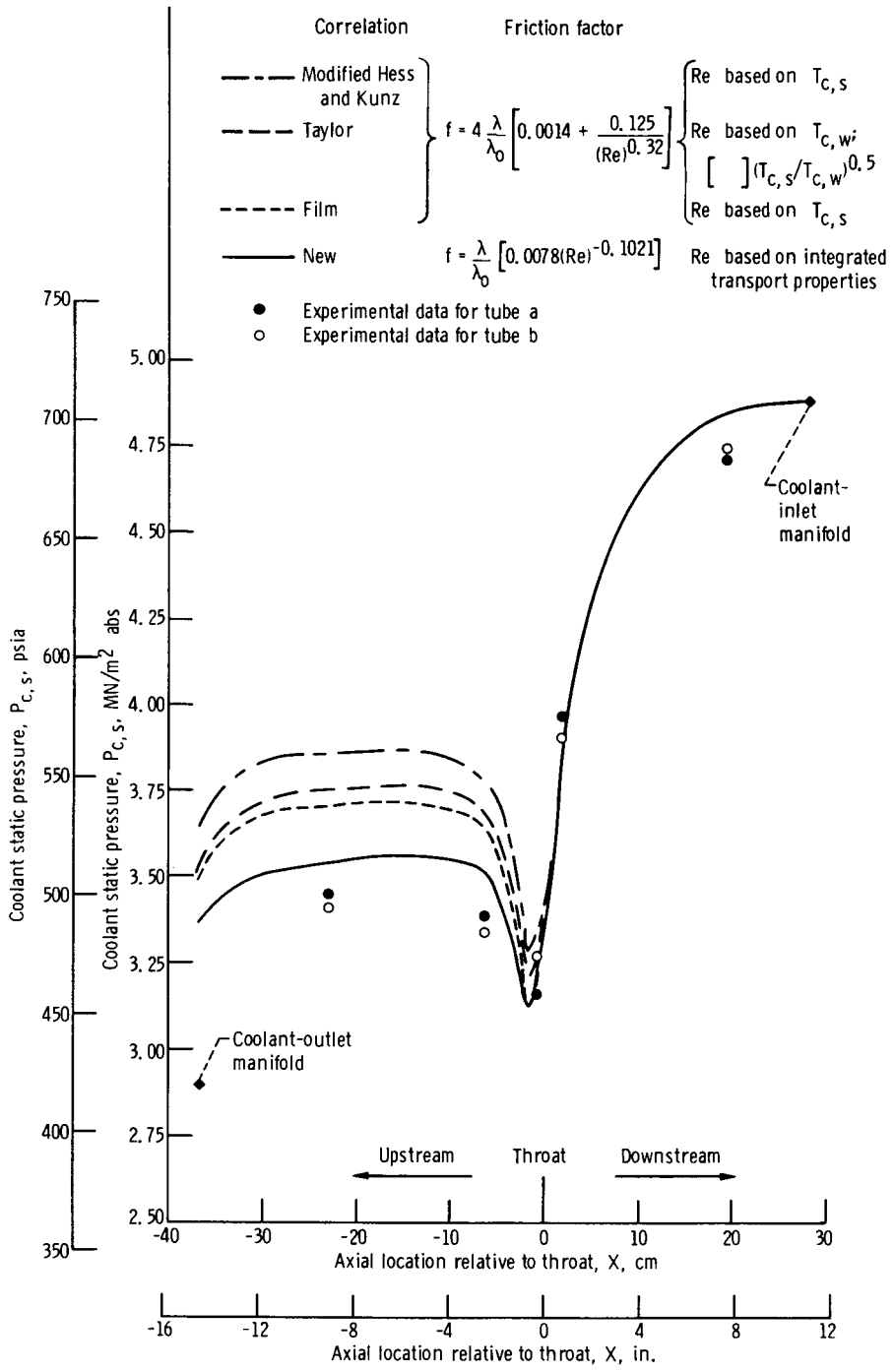

Figure 9. - Measured coolant static pressure as function of axial location for run 91 compared with predictions by various correlations.

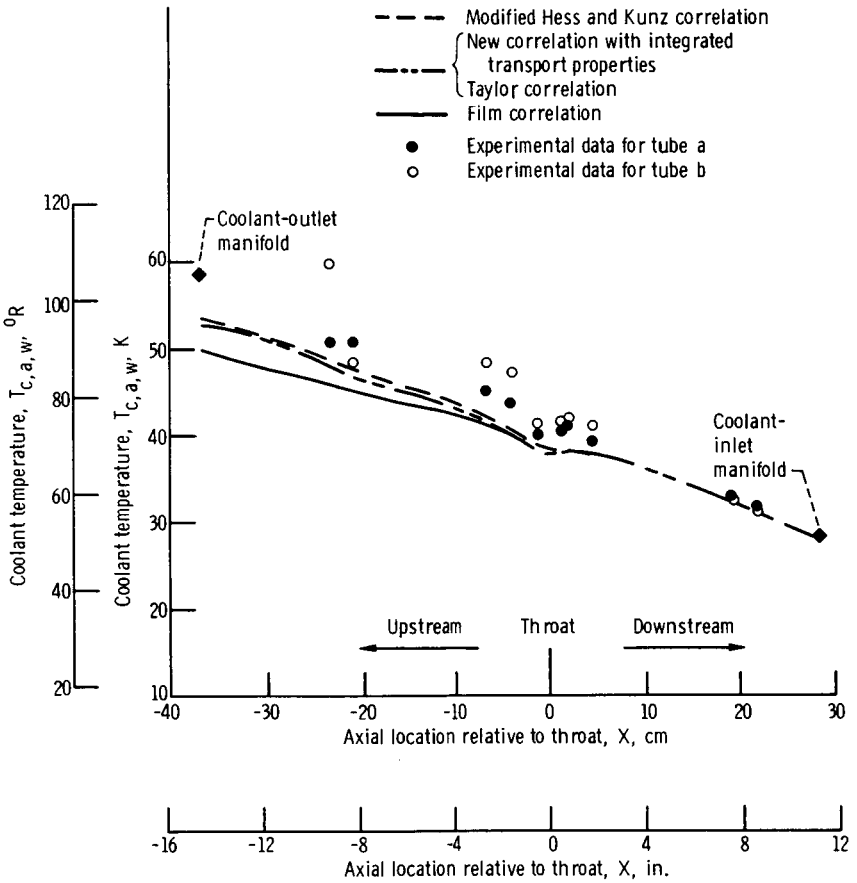

Figure 10. - Measured coolant temperature as function of axial location for run 91 compared with predictions by various correlations.

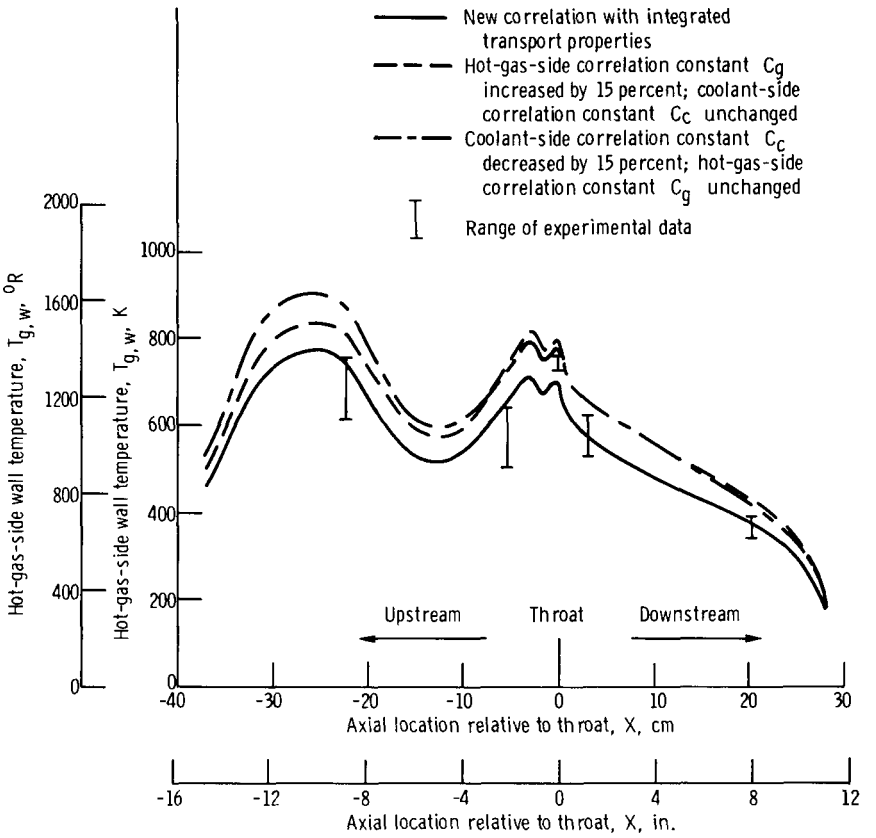

Figure 11. - Effects of changes in correlation constants on hot-gas-side wall temperatures predicted for run 91 by new correlation with integrated transport properties.

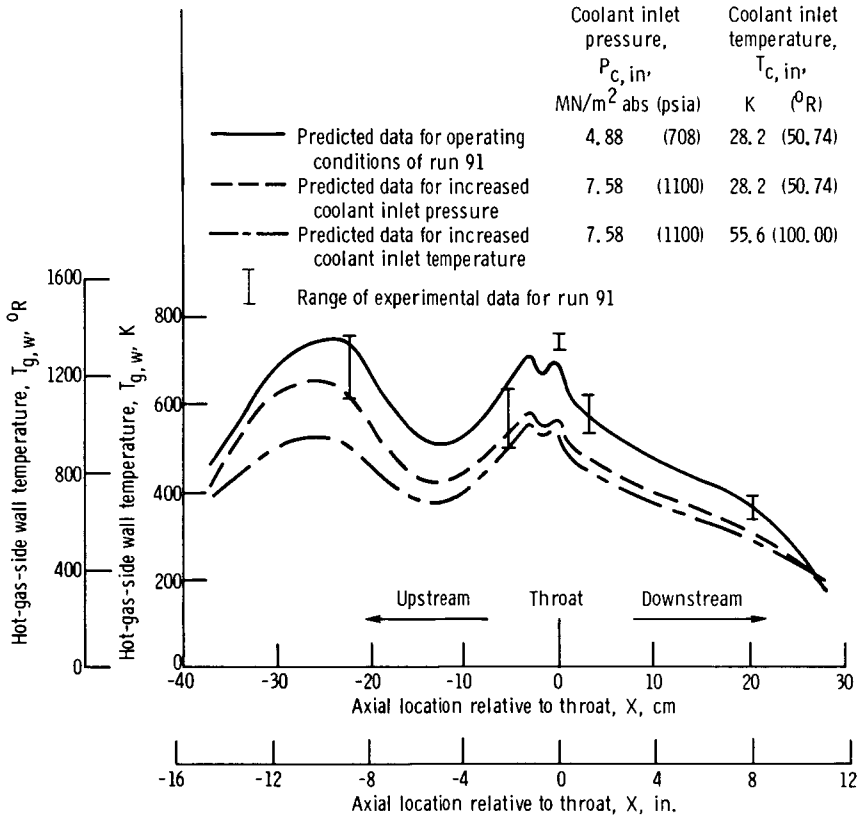

Figure 12. - Effects of changes in coolant inlet pressure and temperature on hot-gas-side wall temperatures predicted by new correlation with integrated transport properties.

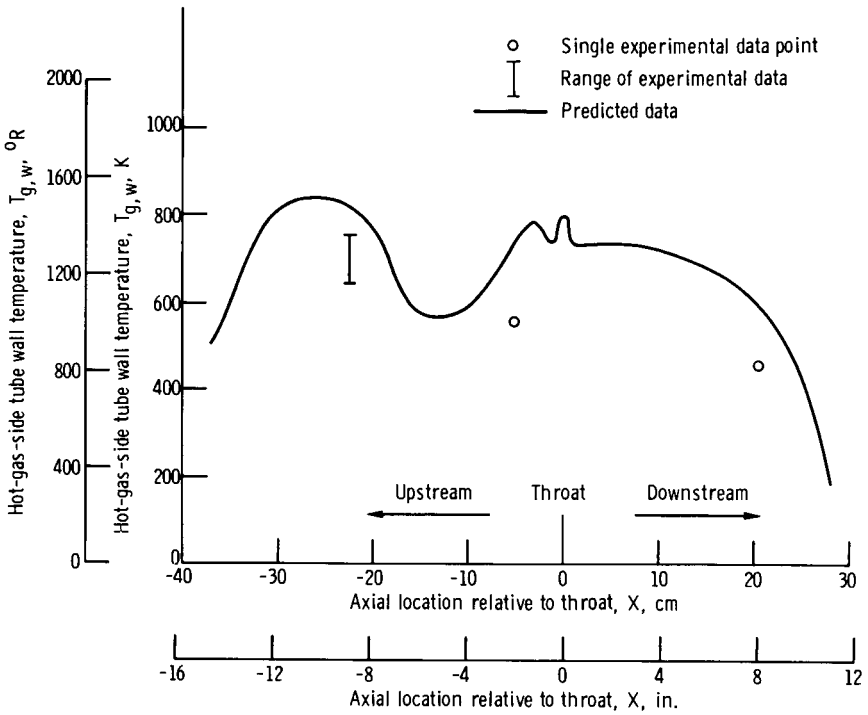

Figure 13. - Predicted and measured hot-gas-side wall temperatures for run 44.

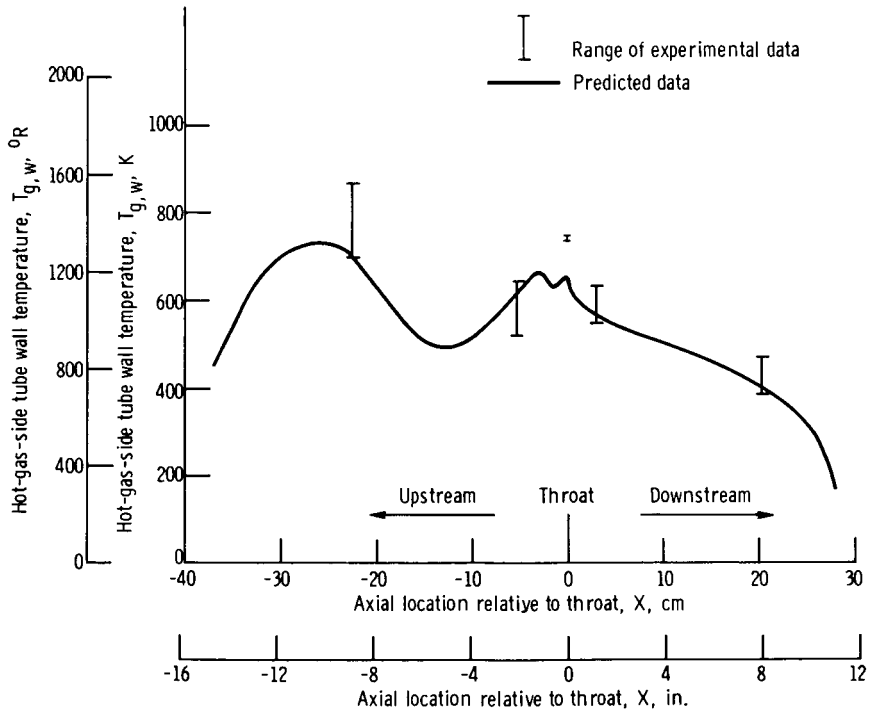

Figure 14. - Predicted and measured hot-gas-side wall temperatures for run 79.

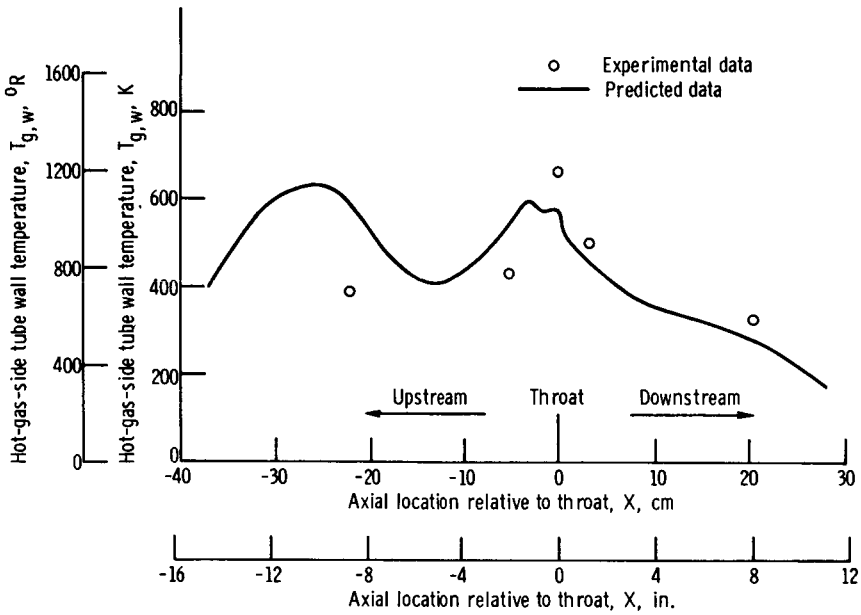

Figure 15. - Predicted and measured hot-gas-side wall temperatures for run 92.

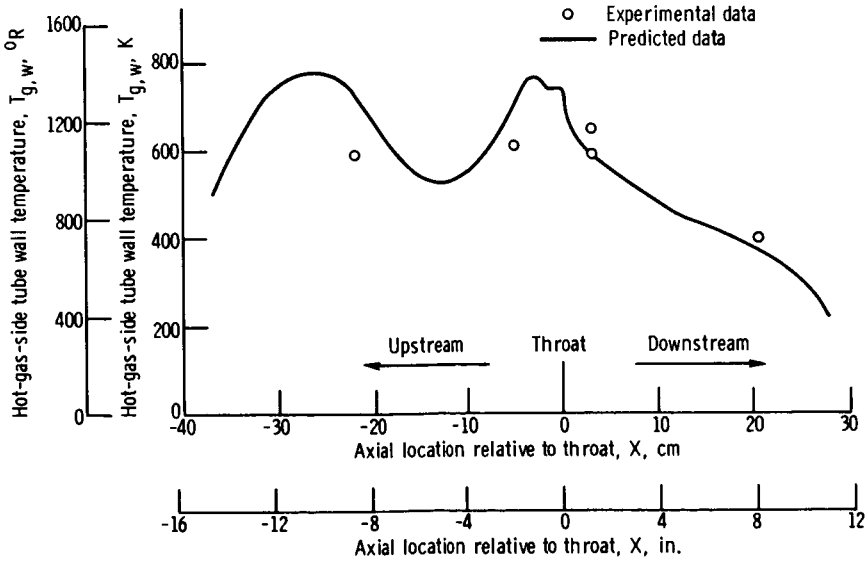

Figure 16. - Predicted and measured hot-gas-side wall temperature for run 94.

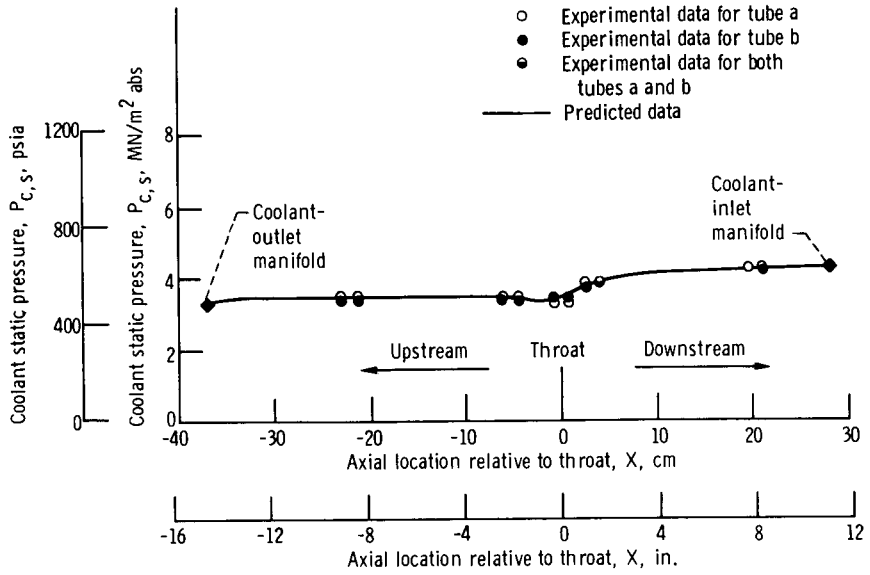

Figure 17. - Predicted and measured coolant static pressures for run 44.

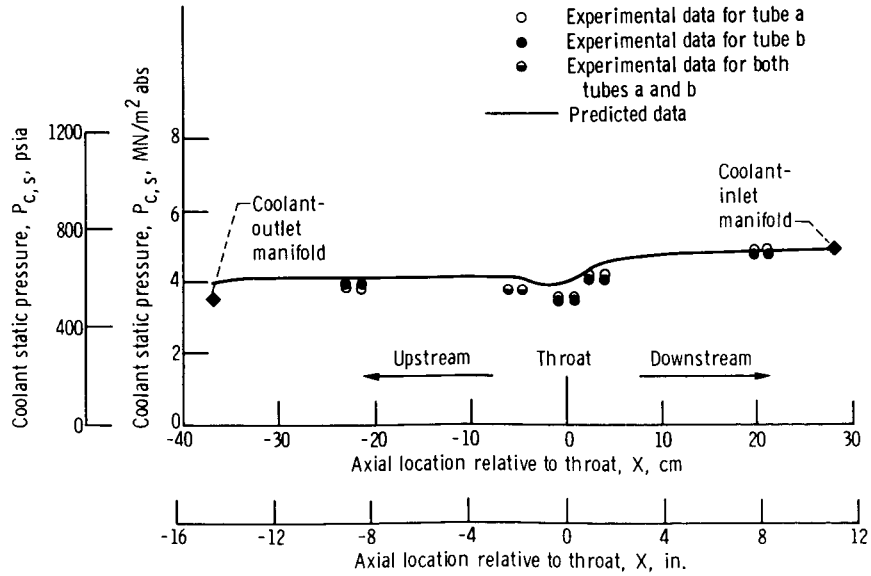

Figure 18. - Predicted and measured coolant static pressures for run 79.

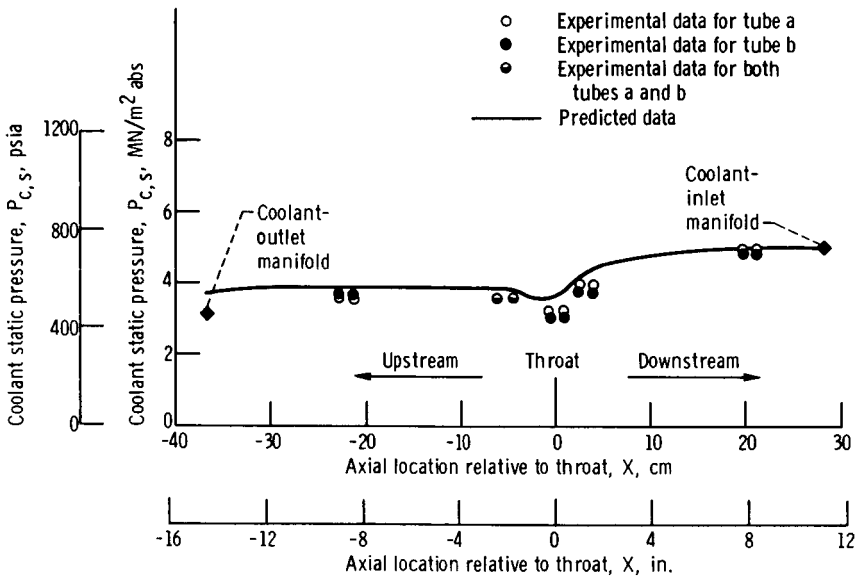

Figure 19. - Predicted and measured coolant static pressures for run 83.

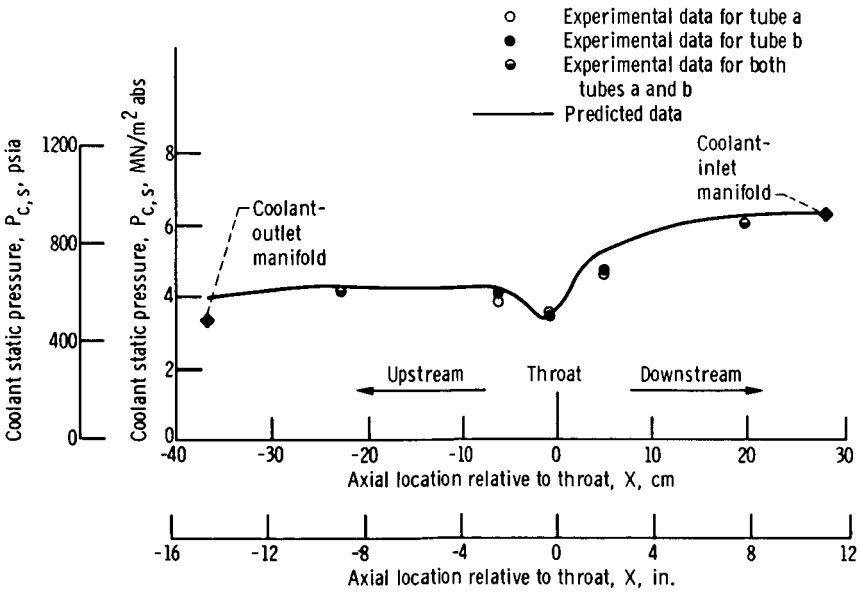

Figure 20. - Predicted and measured coolant static pressures for run 92.

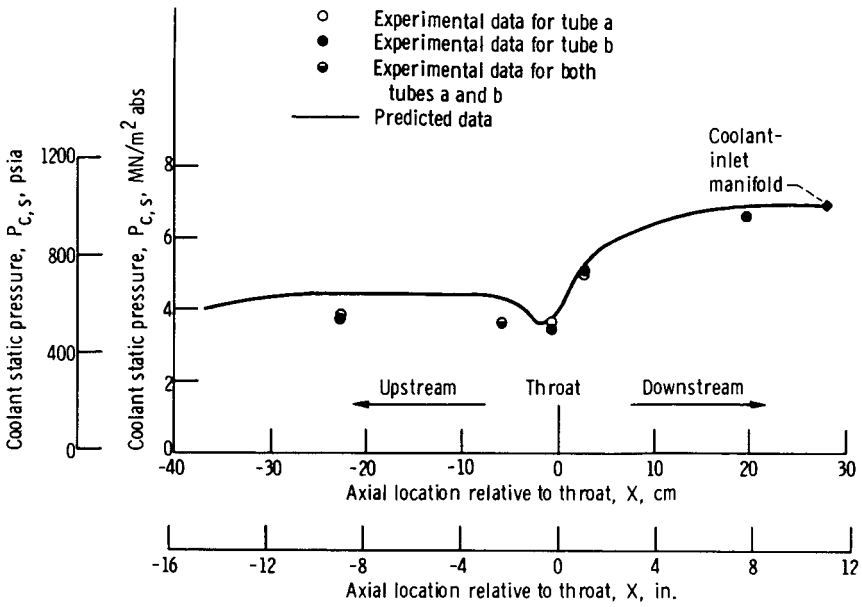

Figure 21. - Predicted and measured coolant static pressures for run 94.

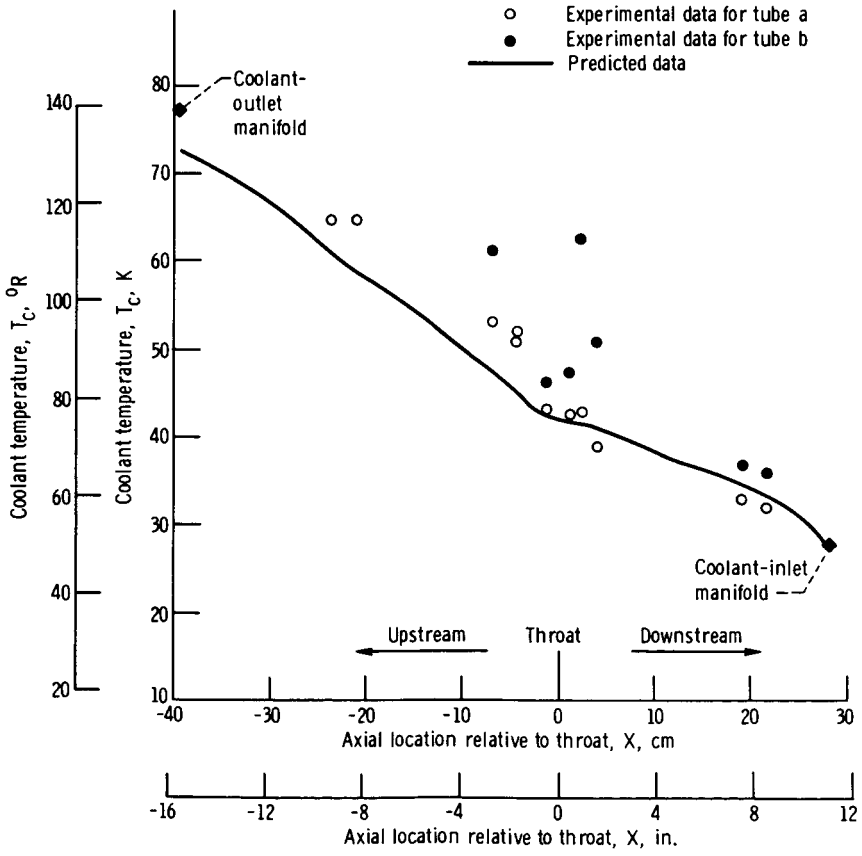

Figure 22. - Predicted and measured coolant temperatures for run 44.

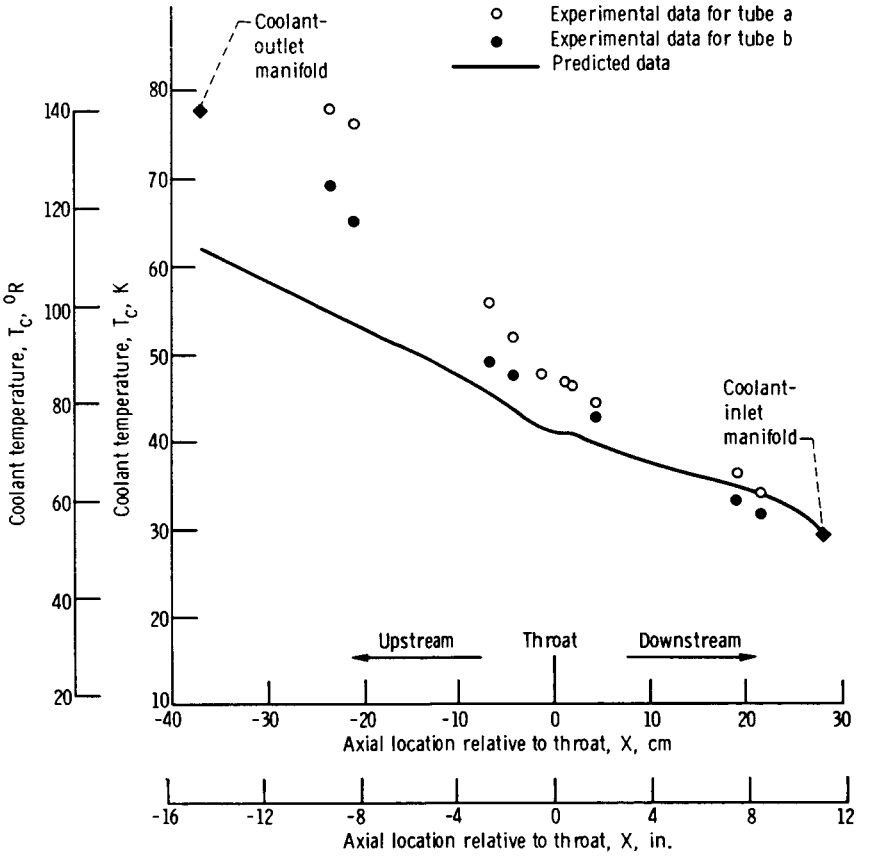

Figure 23. - Predicted and measured coolant temperatures for run 79.

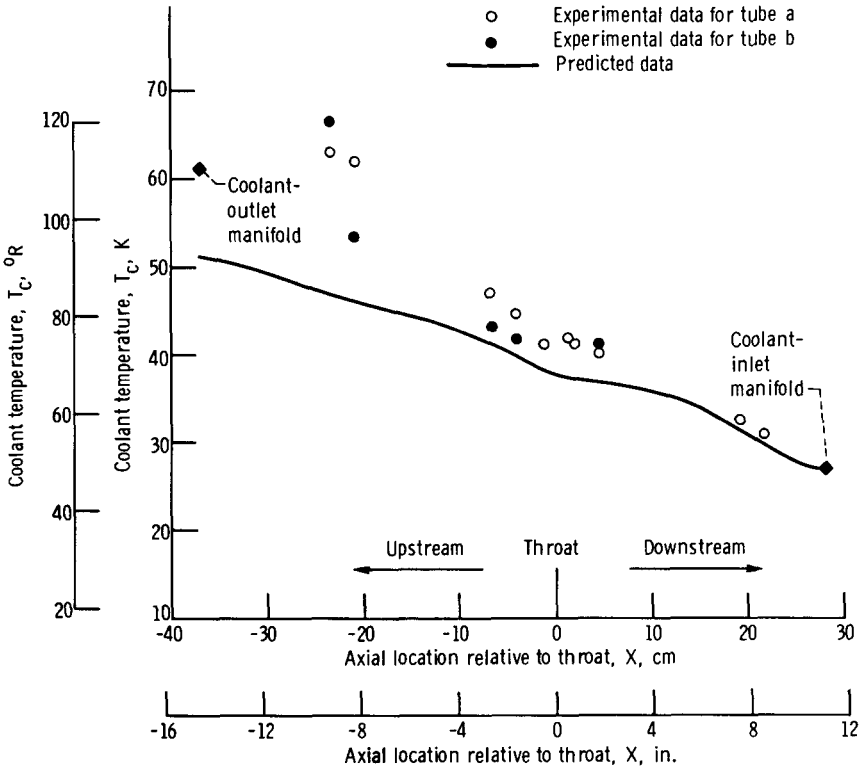

Figure 24. - Predicted and measured coolant temperatures for run 83.

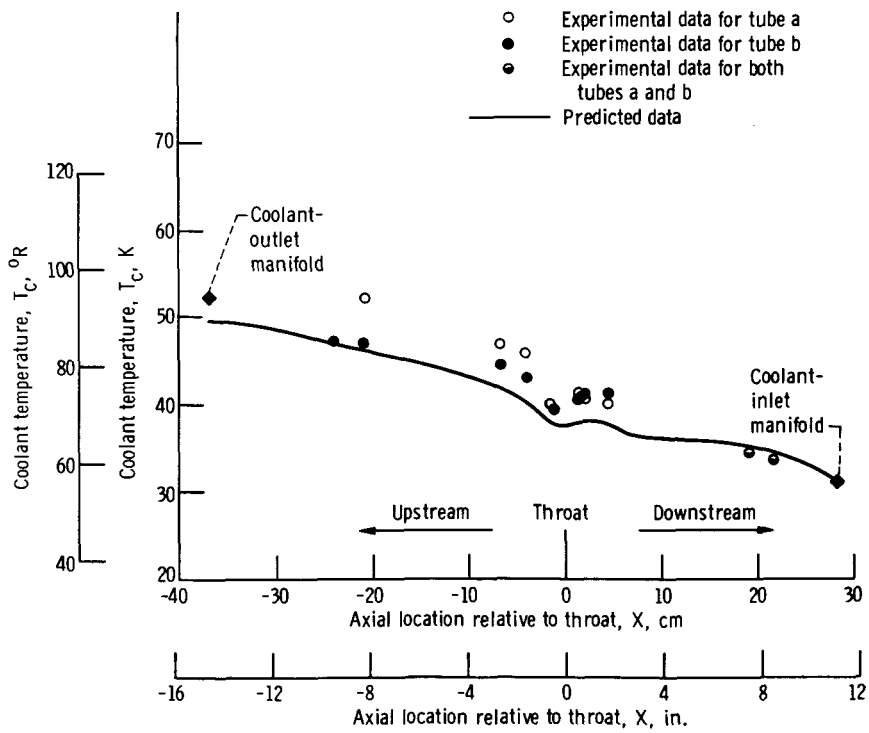

Figure 25. - Predicted and measured coolant temperatures for run 92.

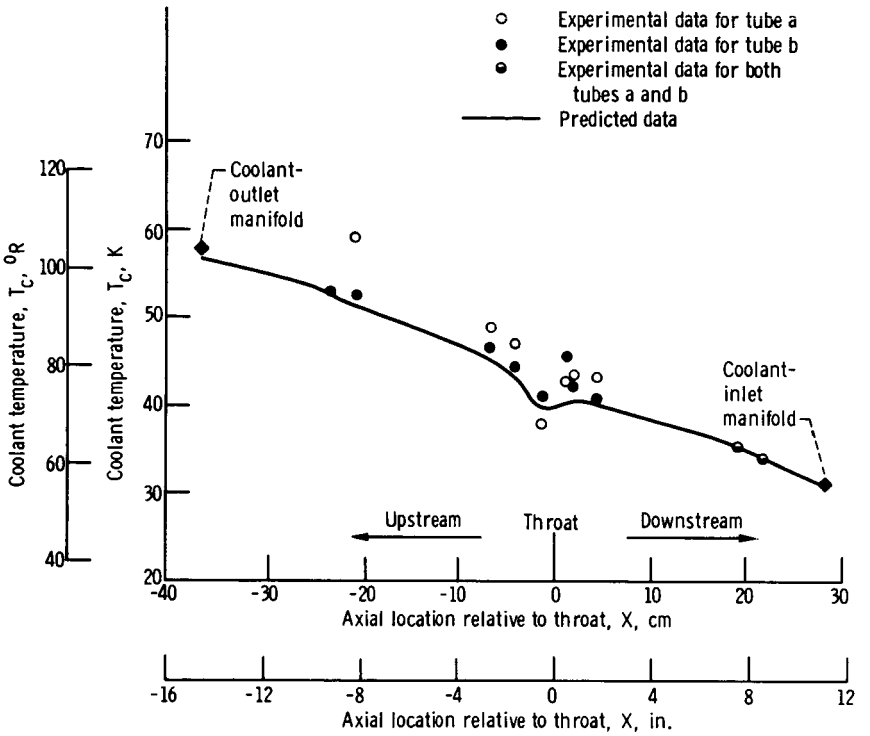

Figure 26. - Predicted and measured coolant temperatures for run 94.

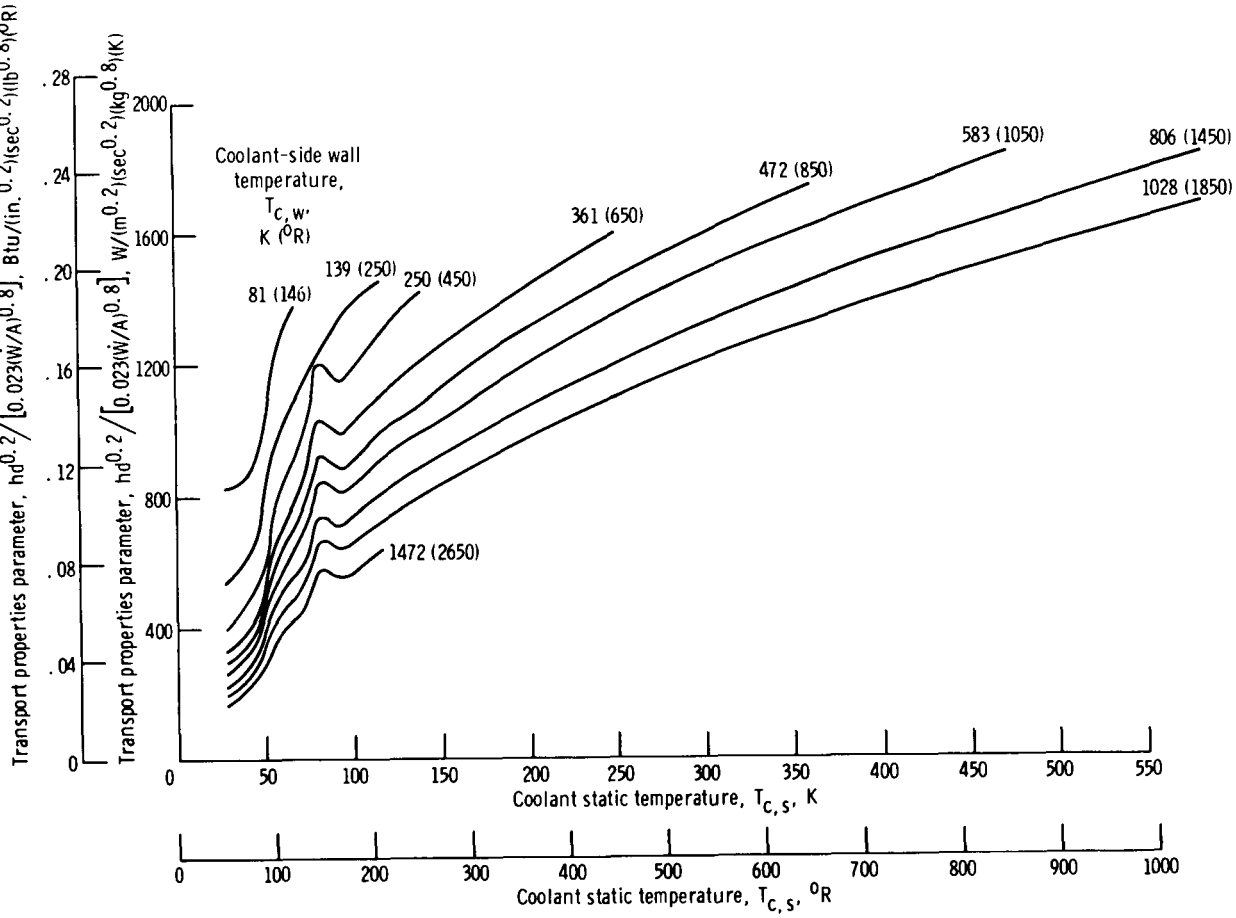

Figure 27. - Transport properties parameter (for properties introduced by integration technique) as a function of coolant static, or bulk, temperature for various coolant-side wall temperatures. Coolant static pressure, 3.447 meganewtons per square meter absolute (500 psia). Transport properties parameter $hd^{0.2}/[0.023(\dot{W}/A)^{0.8}] = (\bar{c}_p\bar{\mu}^{0.2}/\bar{Pr}^{0.6})(\bar{\rho}/\rho_s)^{0.8}$.

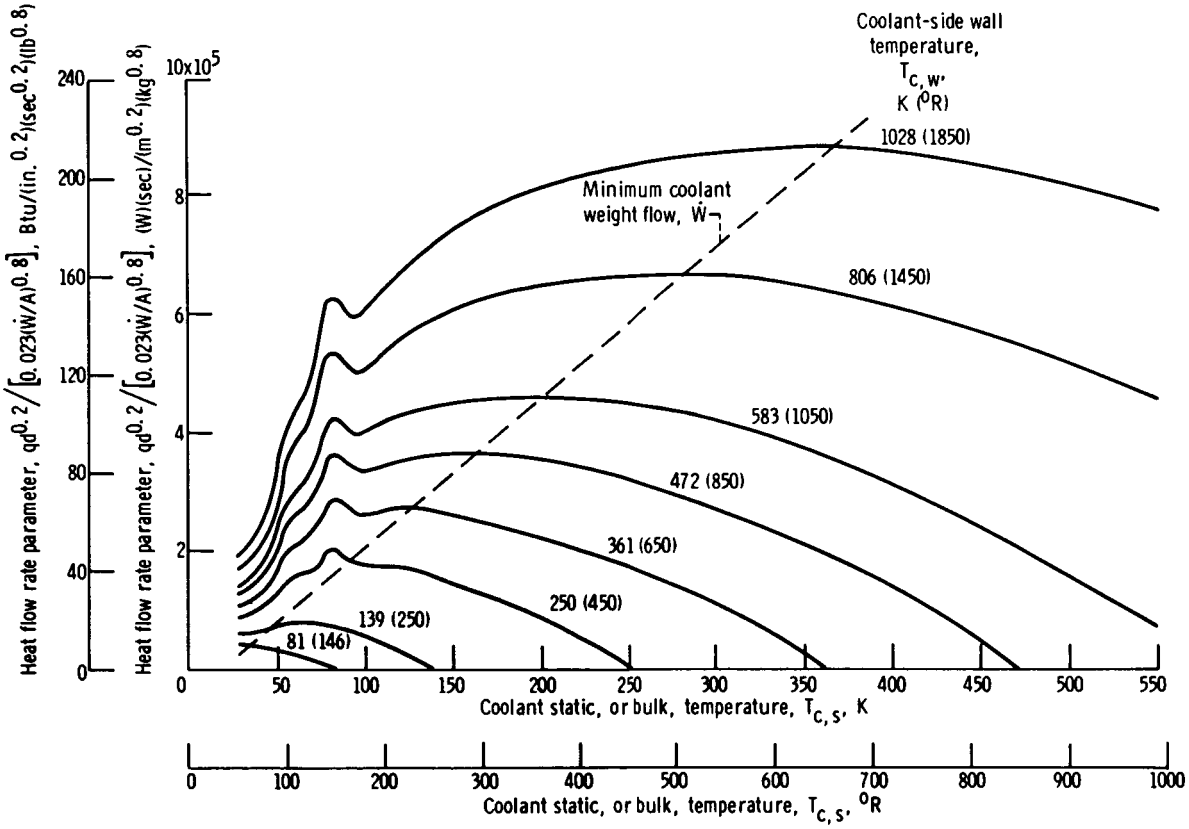

Figure 28. - Heat flow rate as a function of coolant static, or bulk, temperature for various coolant-side wall temperatures. Coolant static pressure, 3.447 meganewtons per square meter absolute (500 psia). Heat flow rate parameter $qd^{0.2}/[0.023(\dot{W}/A)^{0.8}] = (\bar{c}_p\bar{\mu}^{0.2}/\bar{Pr}^{0.6})(\bar{\rho}/\rho_s)^{0.8}(T_{c,w} - T_{c,s})$.

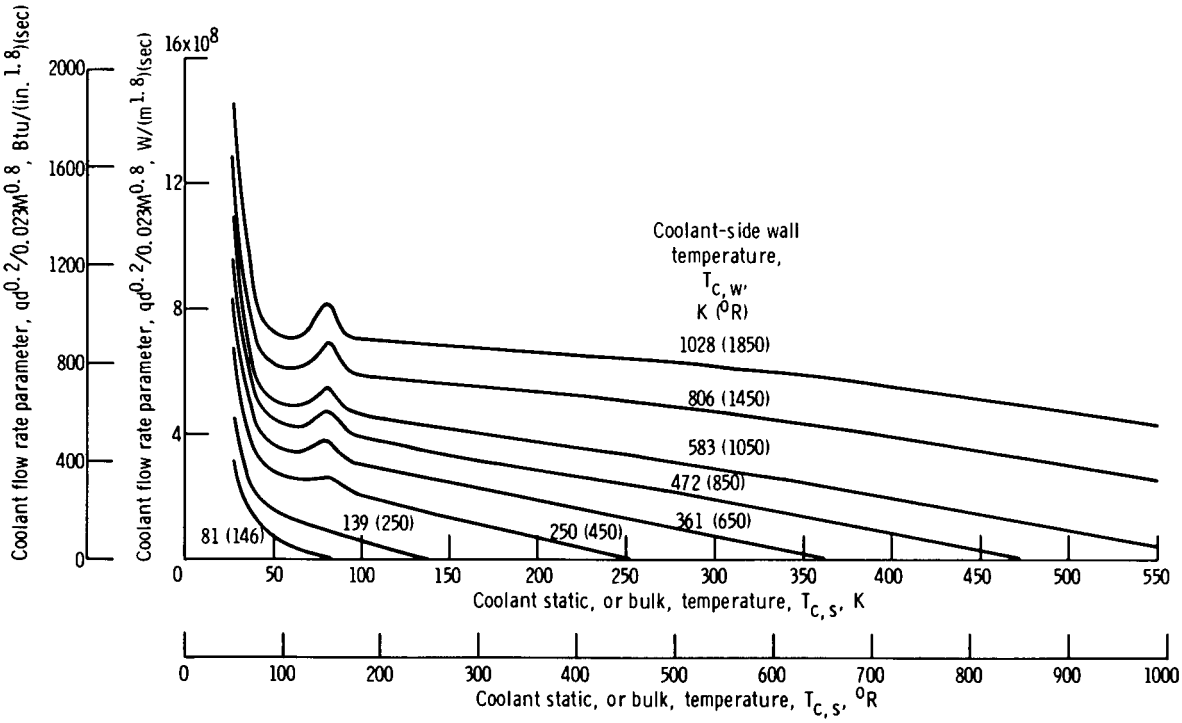

Figure 29. - Coolant flow rate parameter (stressing Mach number or pressure-drop effect) as a function of coolant static, or bulk, temperature for various coolant-side wall temperatures. Coolant static pressure, 3.447 meganewtons per square meter absolute (500 psia). Coolant flow rate parameter $qd^{0.2}/0.023M^{0.8} = (\bar{c}_p\bar{\mu}^{0.2}/\overline{Pr}^{0.6})(\bar{\rho}/\rho_s)^{0.8}(T_{c,w} - T_{c,s})(\rho_s a)^{0.8}$.

NASA-Langley, 1973 —— 33 E-7204